Bioactive Materials 18 (2022) 507–525

Contents lists available at ScienceDirect

Bioactive Materials

journal homepage: www.keaipublishing.com/en/journals/bioactive-materials

Reducing relapse and accelerating osteogenesis in rapid maxillary expansion using an injectable mesoporous bioactive glass/fibrin glue composite hydrogel

Hanjiang Zhao [a,1], Xiangyu Wang [a,1], Anting Jin [a], Minjiao Wang [a], Zeying Wang [a], Xingtai Huang [a], Jiewen Dai [a,**], Xudong Wang [a,***], Dan Lin [a,b,****], Steve GF. Shen [a,b,*]

[a] Department of Oral & Cranio-Maxillofacial Surgery, Shanghai Ninth People's Hospital, Shanghai Jiao Tong University School of Medicine, College of Stomatology, Shanghai Jiao Tong University, National Clinical Research Center for Oral Diseases, Shanghai Key Laboratory of Stomatology & Shanghai Research Institute of Stomatology, Shanghai, 200011, PR China

[b] Shanghai University of Medicine and Health Sciences, Shanghai, 201318, China

ARTICLE INFO

Keywords:
Rapid maxillary expansion
Sutural distraction osteogenesis
Injectable hydrogel
Mesoporous bioactive glass
Bone regeneration

ABSTRACT

Rapid maxillary expansion (RME), as a common treatment for craniomaxillofacial deformity, faces the challenge of high relapse rates and unsatisfactory therapeutic effects. In this study, a standardized Sprague-Dawley (SD) rat RME model was first established with a modified expander as well as retainer design and optimized anterior maxillary expanding force of 100 g which exerted the most synchronized mobility of mid-palatal suture and incisors. Via the standardized model, the high relapse rate was proven to be attributed to insufficient osteogenesis in expanded suture, requiring long-term retainer wearing in clinical situations. To reduce the relapse rate, mesoporous bioactive glass/fibrin glue (MBG/FG) composite hydrogels were developed for an *in situ* minimal invasive injection that enhance osteogenesis in the expanded palate. The component of 1 wt% MBG was adopted for enhanced mechanical strength, matched degradation rate and ion dissolution, excellent *in vitro* biocompatibility and osteoinductivity. Effects of 1%MBG/FG composite hydrogel on osteogenesis in expanded mid-palatal sutures with/without retention were evaluated in the standardized model. The results demonstrated that injection of 1%MBG/FG composite hydrogel significantly promoted bone formation within the expanded mid-palatal suture, inhibited osteoclastogenesis and benefited the balance of bone remodeling towards osteogenesis. Combination of retainer and injectable biomaterial was demonstrated as a promising treatment to reduce relapse rate and enhance osteogenesis after RME. The model establishment and the composite hydrogel development in this article might provide new insight to other craniomaxillofacial deformity treatment and design of bone-repairing biomaterials with higher regenerative efficiency.

1. Introduction

Severe maxillary transverse deficiency (MTD) resulted from congenital malformation (e.g., cleft lip and/or palate) is one of the most pervasive maxillofacial malformation with high clinical demand [1–3]. Rapid maxillary expansion (RME), as the most regular treatment for MTD, has a high relapse rate of the expanded mid-palatal suture due to its inherent tendency of shape recovery and insufficient bone regenerative capability [4–7]. To avoid relapse, current treatments including excessive orthopedic expansion and long-term retainer wearing, mainly aim to resist the recovery tendency and have practical disadvantages and unsatisfactory therapeutic effects [8–10]. Though RME with long-term retention suffice for many mild MTD conditions, high relapse rates are unavoidable in cases of severe MTD including cleft lip and/or

Peer review under responsibility of KeAi Communications Co., Ltd.

* Corresponding author.
** Corresponding author.
*** Corresponding author.
**** Corresponding author.
E-mail addresses: daijiewen@163.com (J. Dai), xudongwang70@hotmail.com (X. Wang), d.lin@foxmail.com (D. Lin), shengf@sumhs.edu.cn (S.GF. Shen).

[1] These authors are joint first authors and contributed equally to this work.

https://doi.org/10.1016/j.bioactmat.2022.03.001
Received 7 July 2021; Received in revised form 24 February 2022; Accepted 1 March 2022

palate due to insufficient bone regeneration. Therefore, we seek to find a minimally invasive treatment that enhance bone regeneration in the expanded palate to reduce the relapse rate of RME with shortened retention time.

To reduce the relapse rate and shorten the retention time, approaches that expedite bone regeneration need to be developed and tested in corresponding animal model that mimics the severe MTD condition. A standardized animal model that can mimic clinical conditions is urgently necessary for treatment improvement and mechanism investigation [5,11–16]. However, RME models in rats were constructed in previous studies with different expansion locations (anterior/posterior) and parameters (expansion force/time and retention time) [17–22]. So far, no systematic comparative study has been reported to determine the RME model parameters for an optimized simulation of severe MTD condition with insufficient bone regeneration. Lack of standardization limits the comparability and further research on RME treatment with this model.

Injectable materials that can be inserted with minimally invasive surgery are acknowledged as a better approach to craniofacial tissue repair [23–33]. Fibrin glue (FG), typically prepared by mixing fibrinogen and thrombin solutions, is commonly used as an injectable tissue repairing hydrogel for its excellent biocompatibility, biodegradability and potential osteogenic capacity [34–41]. However, due to the fast degradation, low mechanical strength and insufficient osteoinductivity of pure FG, numerous researches have been dedicated to introducing inorganic particles (e.g., CPC, HA, β-TCP) into FG hydrogels for mechanical and osteogenic enhancement [42–45]. Mesoporous bioactive glass (MBG), a ternary $CaO–SiO_2–P_2O_5$ bioglass system with ordered mesoporous structure and high specific surface area, is widely used in bone defect repair for its osteoinductivity, osteostimulation, biodegradability and other positive biological effects [46–51]. The introduction of MBG particles into hydrogels has been reported to interact with polymeric matrices and biomolecules to enhance mechanical strength, biological activity and osteogenic efficiency [52–55]. Previous study has demonstrated that bioactive glass coated with FG enhanced bone formation through promoting cell adhesion and early differentiation of osteogenic cells [56]. Therefore, MBG was selected to enhance the mechanical, biological and osteogenic capacity of the injectable FG hydrogel, and MBG/FG composite is expected to combine the merits of both components.

In this work, a standardized rat model of RME was first established with optimized mechanical parameters and modified retainer design. Injectable MBG/FG composite hydrogels were developed in different MBG proportion ranging from 0.5% to 4%, and the *in vitro* physicochemical, mechanical and biological properties were evaluated to optimize the fabrication parameters. On these bases, MBG/FG composite hydrogel was injected *in situ* to promote sutural distraction osteogenesis (DO) and reduce relapse in mid-palatal sutures in the standardized rat RME model, and its regenerative efficiency was validated (Scheme 1).

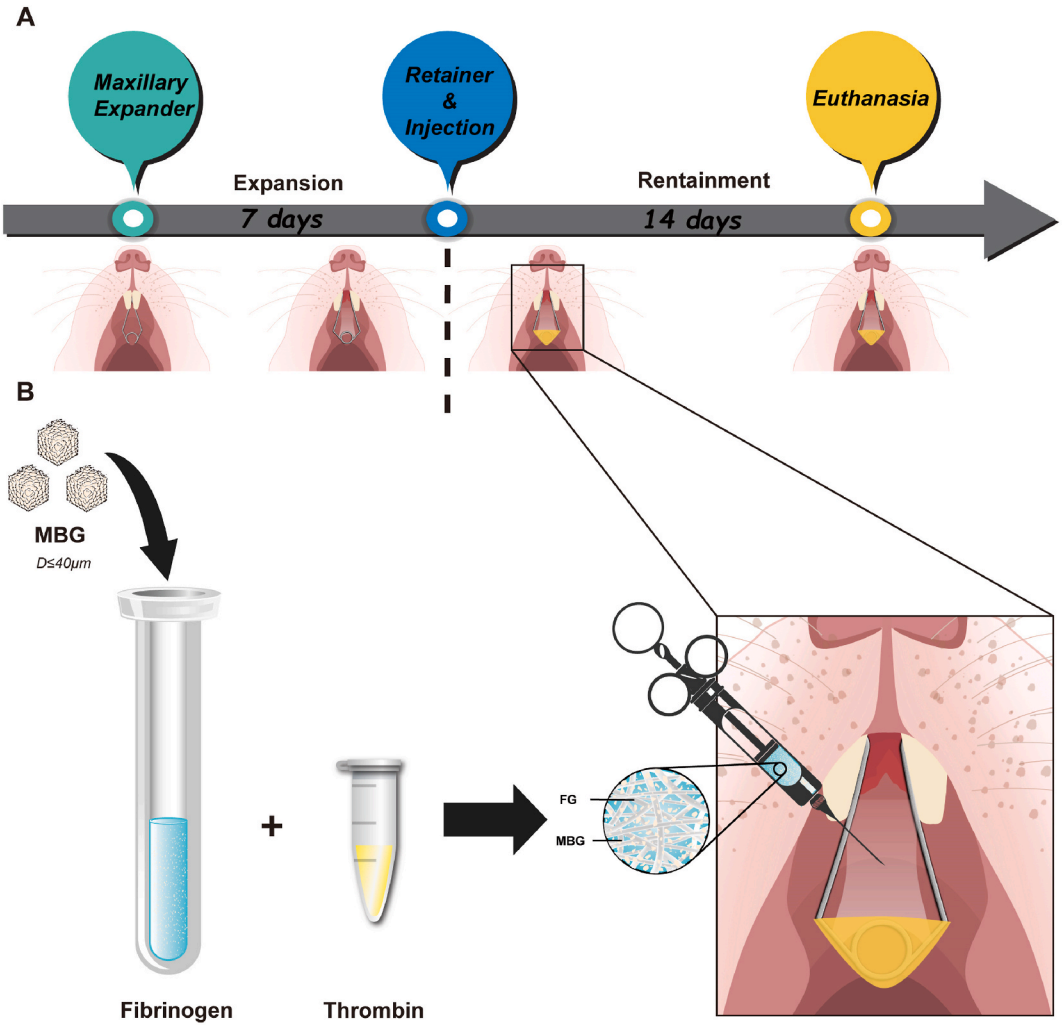

Scheme 1. Schematic illustration of this study: (A) Timeline of the rat RME model establishment; (B) Preparation of MBG/FG composite hydrogel and *in situ* injection in the expanded mid-palatal suture to enhance bone regeneration and reduce the relapse rate after RME.

2. Methods

2.1. Materials

α-MEM culture medium, Fetal bovine serum (FBS), Penicillin-Streptomycin and phosphate buffered saline (PBS) were from Gibco® (Thermo Fisher Scientific Inc. MA, USA). Pluronic® F-127 ($EO_{106}PO_{70}EO_{106}$), fibrinogen, thrombin, fluorescein isothiocyanate-phalloidin (FITC-phalloidin) and DAPI were from Sigma-Aldrich (St. Louis, MO, USA). Cell Counting Kit-8 (CCK-8) was purchased from Dojindo (Shanghai, China). BCA protein assay kit and BCIP/NBT alkaline phosphatase color development kit were from Beyotime Biotech (Jiangsu, China). RNAiso Plus, PrimeScript RT reagent kit and TB Green™ Premix Ex Taq™ were from Takara (Tokyo, Japan). Chemical reagents used for MBG synthesis including tetraethyl orthosilicate (TEOS), $Ca(NO_3)_2{\cdot}4H_2O$ and triethyl phosphate (TEP) were from Sinopharm Group Co. Ltd. (Shanghai, China). Histological reagents including 4% paraformaldehyde and 10% EDTA (0.1 M, pH 7.1) solution were from Servicebio Technology (Wuhan, China).

2.2. Establishment of standardized rat RME model

2.2.1. Design of expander and retainer

Maxillary anterior expander for rats was an improved design based on previous studies [5]. 0.014-inch stainless steel wire was bent into a helical spring (φ 2 mm) with bilateral curve-ended expanding arms which provided expanding force (Fig. 1A). The expanding force were adjusted via different bending angles on the expanding arms. Each expander was calibrated using a force gauge (Tention gauge T-200, TOKK, Japan, error range ±5 g) to 50 g, 75 g, 100 g and 125 g of force.

After expansion, the expander was deactivated and modified into a retainer by cementing with light-cure acrylic resin (Transbond Supreme LV Low Viscosity Light Cure Adhesive, 3 M Unitek, USA) from helical spring to bending angle to remove the elastic strain.

2.2.2. Procedure of maxillary expansion, retention and hydrogel injection

6-week-old male Sprague-Dawley (SD) rats (average weight: 200 ± 10 g) were anaesthetized with 4–5% isothesia isoflurane gas (RWD Life Science, China). Prior to placing the expander, a tiny gap was created at the gum margin of the incisors by a slow-speed dental handpiece (Fig. 1B, b2). The curved ends of the expander were wrapped around each incisor through the gap, with the helical spring tightly appressed the palatine papillae. Then the expander was cemented onto the incisors with light-cure acrylic resin (Fig. 1B, b3). The expansive force was continuously delivered from incisors to the mid-palatal suture for 7 days. For optimization of expanding force, 15 SD rats were divided into five groups (n = 3 for each group): sham surgery, 50 g, 75 g, 100 g and 125 g; and the rats were euthanized after 7-day expansion to obtain the craniomaxillary specimens for further imageological and histological inspection.

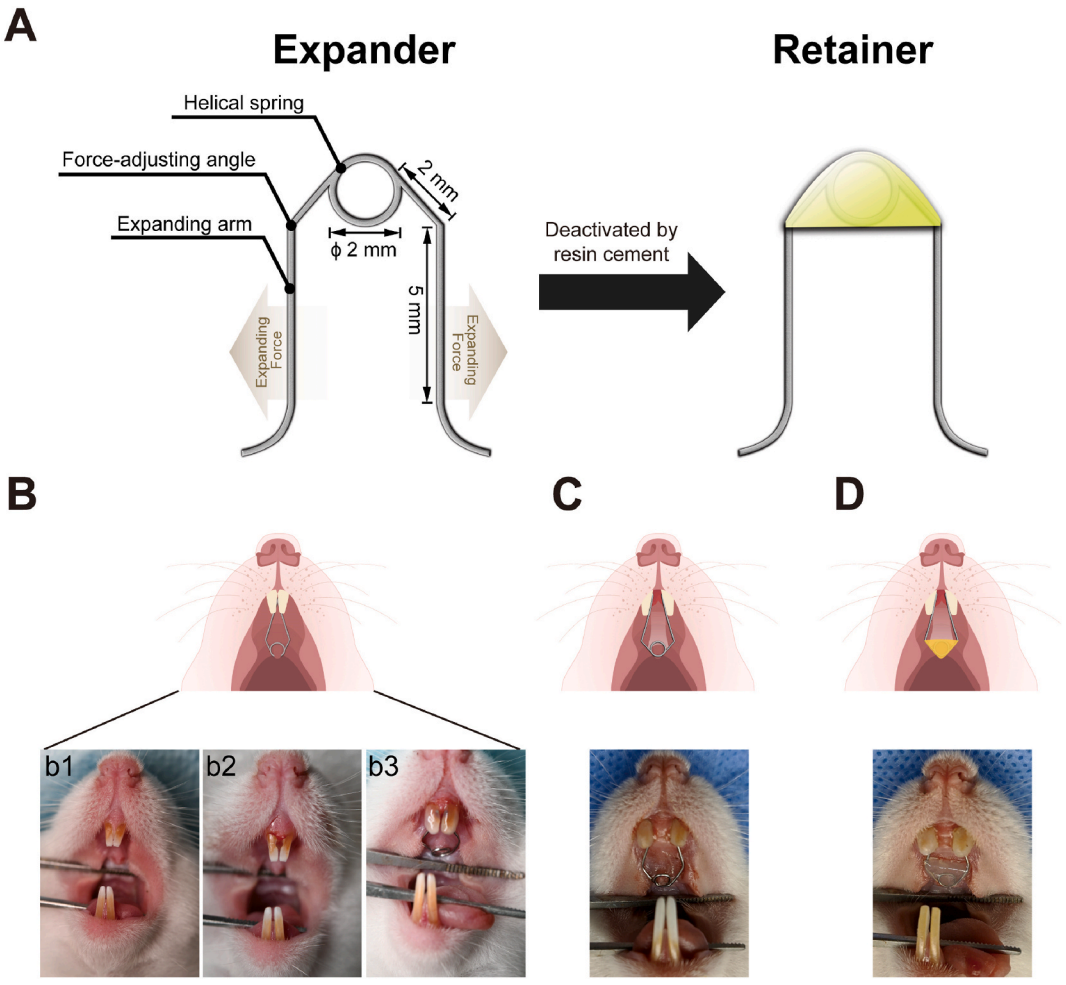

Fig. 1. Design of a modified maxillary expander/retainer for the SD rat RME model. (A) The expander consisted of a helical spring (φ 2 mm) and bilateral curve-ended expanding arms with force-adjusting angles, deactivated by cementing with resin to form a retainer. (B) Preparation for maxillary expansion: b1. Pretreatment; b2. creation of a tiny gap at gum margin of incisors; b3. curved ends of the expander wrapped around incisors through the gap. (C) Expanded incisors after expansion for 7 days. (D) Retainer deactivated with resin.

After 7-day expansion, the expanders were deactivated and modified into retainer as above-mentioned in 2.2.1. To investigate the relationship between relapse and retention time, 9 SD rats were divided into three groups (n = 3 for each group): no retention, 7-day and 14-day retention; the maxillae were *in vivo* imaged with micro-CT for distance measurement, then the expander/retainer was removed for 7 days before euthanasia to observe relapse via further imageological and histological inspection.

To reduce relapse and enhance osteogenesis, after 7-day expansion, the maxillae were *in vivo* imaged with micro-CT for distance measurement, then 96 μL 1% MBG/fibrinogen solution and 4 μL thrombin solution were sequentially injected into the expanded palatal suture for *in situ* gelation of 1%MBG/FG hydrogel. 24 SD rats were divided into 4 groups (n = 6 for each group): Ctrl, retention, injection, retention+injection; all 4 groups of rats underwent 14-day treatment before euthanasia.

All animal experiments were performed in compliance with the guidelines developed by the Institutional Animal Care and Use Committees of Shanghai Ninth People's Hospital, and the protocols were reviewed and approved by the Ethic Committee of Shanghai Ninth People's Hospital. All animals were kept in a 12-h light and dark environment at a constant temperature of 23 °C and fed an ordinary, solid diet and water ad libitum. At the end of each experiment, the animals were euthanized by anesthetic overdose to obtain the maxillae.

2.2.3. Micro-CT analysis

Microcomputed tomography (micro-CT; PerkinElmer Quantum GX, USA) of the craniomaxillary specimens was performed to measure the expansion/relapse distance and evaluate the bone formation within the expanded mid-palatal suture.

1) Distance measurement and calculation of relapse ratio

The palatal expansion/relapse distances were measured via *in vivo* imaging, with the animals anaesthetized with 4–5% isoflurane gas. The scanning voltage and current was set at 90 kV and 88 μA, respectively, with a field of view (FOV) of 45 mm, voxel size of 90 μm, scan mode "High Resolution" and scanning time of 4 min. Then the data were reconstructed with 15.4 mm FOV and 30 μm voxel size for distance measurement.

With the sagittal plane through the center of mid-palatal suture, coronal plane through the center of incisors and horizontal plane located in the middle of the maxillary, the expanded distances of suture/teeth were measured in the two-dimensional image of horizontal plane at two time points (T_1 and T_2). The skeletal/dental relapse ratio between the two time points was calculated according to the following formula:

$$Relapse\ ratio = \frac{T_2 - T_1}{T_1} \times 100\%$$

2) Evaluation of bone formation

Bone formation in the expanded mid-palatal suture was evaluated via *in vitro* imaging. The scanning voltage of 90 kV and current of 88 μA were applied, with a field of view (FOV) of 25 mm, voxel size of 50 μm scan mode "High Resolution" and scanning time of 14 min. The data were reconstructed with 12.8 mm FOV and 25 μm voxel size and then analyzed with the software Analyze 12.0 (PerkinElmer, USA) with the threshold range of 3000/8500 (min/max) to isolate the bone tissue from the soft tissue. The expanded palatal sutures were selected as region of interests (ROI) for quantification of bone mineral density (BMD) and bone volume/total volume (BV/TV).

2.2.4. Histology and immunohistochemistry

The samples were fixed with 4% paraformaldehyde, decalcified in 10% EDTA and dehydrated using Automatic dehydrator (HistoCore PEARL, Leica, Germany). 5 μm thick sections were sliced by a rotary microtome (RM2255, Leica, Germany), deparaffined and stained with hematoxylin and eosin (H&E) and Masson's trichrome. TRAP staining was adopted to examine the osteoclast formation using a commercial kit (G1050-50T, Servicebio, China).

Immunohistochemical staining of osteocalcin (OCN), CD31, RANKL and OPG were performed. Primary antibodies of OCN (GB11233, Servicebio, China), CD31 (GB11163-2, Servicebio, China), RANKL (GB11235, Servicebio, China), and OPG (GB11151, Servicebio, China) were diluted according to manufacturer's instruction. Briefly, after deparaffinage, antigen retrieval was carried out via water-bath heating with 10 mM sodium citrate buffer. The sections were blocked for 30 min in 10% blocking serum and incubated overnight at 4 °C with primary antibody. Then the sections were incubated with goatradish-peroxidase-conjugated rat secondary antibody (GB23303, Servicebio, China) and 3,3′-diaminobenzidine tertrahydrochloride (DAB; DAKO, Agilent, USA) for color development. The sections were then counterstained with hematoxylin and mounted.

All histologic sections were scanned with PANNORAMIC DESK/MIDI/250/1000 (3DHISTECH, Hungary) and viewed with Caseviewer 2.4 (3DHISTECH, Hungary). Immunohistochemical sections were analyzed by Image-pro plus 6.0 (Media Cybemetics, USA).

2.2.5. Sequential fluorescent labeling and VG staining

Briefly, 20 mg/kg calcein (CA) and 30 mg/kg alizarin red (AR) were intraperitoneally injected at day 7 (initial retention) and day 14 (7-day retention) respectively. The obtained samples were fixed in 4% paraformaldehyde for 5 days, and then dehydrated with gradient ethanol for 10 days. After dehydration, the samples were infiltrated into Technovit® 7200 VLC resin for 30 days and finally embedded in it with photocuring. The encapsulated samples were cut into ~150 μm thick slices with a diamond band saw (EXAKT, Germany). Then the slices were ground and polished to a final thickness of ~50 μm. Fluorescent labeling of the specimens were observed under confocal laser scanning microscopy (Leica, Germany). The excitation/emission wavelengths of the fluorophores were 488/517 nm (CA) and 543/617 nm (AR). The rate of mineralization in mid-palatal suture was determined by measuring the distance between two corresponding fluorescent stripes while the fluorescence-labeled areas were quantified to reflect the bone formation during the corresponding periods. The graphic quantifications were analyzed by Image J. After fluorescent observation, the slices were stained with Van Gieson's picro fuchsin (VG) to observe the mineralized mid-palatal suture tissue.

2.3. Material preparation and characterization

2.3.1. MBG particles

MBG was prepared by a modified templating method with F127 as mesoporous template as previously reported [46,47]. Briefly, 4.0 g of F127, 1.0 g of HCl (1 M), 0.76 g of $Ca(NO_3)_2{\cdot}4H_2O$, 0.23 g of TEP and 5.2 g of TEOS were dissolved in 50 g of ethanol and stirred at 40 °C for 24 h. The resulting solution was rotary evaporated under vacuum condition at 60 °C for 30min to achieve a viscous concentrated sol, dried on watchglass at 60 °C for 3 days, followed by a calcination program (600 °C for 5 h, ramp of 1 °C/min) to remove the organic template. The calcinated MBG was then ground and sieved through a 400-mesh screen obtain the final MBG particles.

2.3.2. FG and MBG/FG composite hydrogels

Fibrin glue (FG) was formed by mixing 5 mg/mL fibrinogen solution and 100U/mL thrombin solution at a volume ratio of 24:1.

To fabricate an MBG/FG composite hydrogel, MBG particles were added in the 5 mg/mL fibrinogen solution at the ratio of 0.5 wt% to 4 wt % before mixture with thrombin solution. Hydrogels with different MBG amount will be referred to as FG, 0.5%MBG/FG, 1%MBG/FG, 2%MBG/FG and 4%MBG/FG respectively in the following article.

For *in vitro* experiments, 240 μL fibrinogen solution and 10 μL thrombin solution were mixed and *in situ* gelled in the bottom of 24-well plate. For physicochemical and mechanical characterization, hydrogels were prepared with φ 6.5 mm cylinder moulds.

2.3.3. Physicochemical characterization

The surface morphologies of the FG and MBG/FG composite hydrogels were observed by scanning electron microscopy (SEM; S-4800, Hitachi, Japan). The ordered mesoporous structure of MBG particles was observed by transmission electron microscope (TEM; JEM-2100F, JEOL, Japan). Mesoporous size distribution was analyzed with Brunauer-Emmet-Teller (BET) by Micrometrics porosimeter (ASAP2010 N, Micrometrics Instrument, USA). Element composition of MBG was analyzed by energy dispersive spectrometry (EDS; Falcon, USA). Phase composition and crystal structural parameters of MBG were characterized by wide-angle and small-angle X-ray diffraction (XRD; Rigaku D/max 2550VB/PC, Japan).

2.3.4. Mechanical strength

Compressive strengths of the hydrogels were measured using a universal testing machine (HY-1080, Shanghai Hengyi Testing Machine Co. Ltd., China). For each sample, at least three specimens were tested, and the results were averaged.

2.3.5. Degradation and dissolution rate

In vitro degradation of the hydrogels was evaluated in PBS solution. 250 μL hydrogel was immersed in 1 mL PBS in a shaker incubator (37 °C, 100 rpm). At each time point (2/4/6/8/10/12/14 days), the degradation liquor was collected and the residual hydrogels were weighed in a high-precision electronic balance before adding fresh PBS to continue degradation. Ca^{2+} and SiO_4^{4-} concentrations in the degradation liquor of different time points were determined by inductively coupled plasma-atomic emission spectroscopy (ICP-AES, IRIS 1000, Thermo Elemental, USA) to profile the ionic dissolution of MBG.

2.4. In vitro biological evaluation

2.4.1. Cytotoxicity, proliferation, and adhesion

Rat bone marrow mesenchymal stem cells (rBMSCs) were extracted from rat bone marrow and cultured in α-MEM supplemented with 10% FBS and 1% penicillin-streptomycin in a 5% CO_2 incubator at 37 °C. Passage 3–5 of rBMSCs were utilized for the *in vitro* experiments in this study.

Cytotoxicity and cell proliferation were evaluated by CCK8 assay. In brief, rBMSCs were co-cultured with FG and MBG/FG composite hydrogels in 24-well plates at a density of 2×10^4 cells/well. After 4 and 7 days of culture, CCK-8 (reagent: culture medium = 1:10) was added into each well and cultured at 37 °C for 1 h. Then the mixture was extracted and quantified by the absorbance of 450 nm on a plate reader (Biotek Epoch, USA).

For cell adhesion observation, rBMSCs were co-cultured with FG and MBG/FG composite hydrogels in 24-well plates at a density of 5×10^4 cells/well. After 24 h of incubation, the cells were fixed with 4% glutaraldehyde, stained with FITC-phalloidin and DAPI, and observed under confocal laser-scanning microscopy (CLSM; Leica TCS SP5, Germany).

2.4.2. ALP staining and ALP activity assay

For ALP staining and activity quantification, rBMSCs were co-cultured with FG and MBG/FG composite hydrogels in a 24-well plate at a density of 5×10^4 cells/well. After 24 h, the medium was changed to osteoinductive medium (α-MEM containing 2% FBS, 0.05 mM ascorbic acid, 100 mM β-glycerol phosphate and 100 nM dexamethasone). After osteoinduction for 4/7 days, ALP staining was performed using a BCIP/NBT alkaline phosphatase color development kit (Beyotime, Jiangsu, China) according to the manufacturer's protocol. For ALP activity quantification, the medium was removed and 1% NP-40 solution was added and incubated for 1h to obtain cell lysates. Then 50 μL of the cell lysates from each sample was pipetted to a new 96-well plate. 200 μL of 1 mg/mL pNPP-Na solution containing 0.1 mol/L glycine and 1 mmol/L $MgCl_2 \cdot 6H_2O$ was added and incubated for 30 min at 37 °C. ALP activity was quantified by the absorbance of 405 nm using a microplate reader (Biotek Epoch, USA). Total protein content of each cell lysate was determined using a BCA protein assay kit (Beyotime, Jiangsu, China). ALP levels were normalized with total protein content, and the experiments were performed in triplicates.

2.4.3. Alizarin red S staining

For ALP staining and activity quantification, rBMSCs were co-cultured with FG and MBG/FG composite hydrogels in a 24-well plate at a density of 5×10^4 cells/well. After 24 h, the medium was changed to osteoinductive medium. After cultured in osteoinductive medium for 14 and 21 days, cells were fixed in 4% paraformaldehyde and stained with Alizarin Red S.

2.4.4. Quantitative real-time (RT)-PCR

Osteogenic and chondrogenic gene expressions of rBMSCs were measured on day 7 by a real-time quantitative reverse transcription-polymerase chain reaction (RT-qPCR) system (Roche LightCycler96, Basel, Switzerland). Briefly, rBMSCs were co-cultured with FG and MBG/FG composite hydrogels in a 24-well plate at a density of 5×10^4 cells/well. After 24 h, the medium was changed to osteoinductive medium. After 7 days of culture, RNA was extracted from cells and reverse transcribed into complementary DNA (cDNA) using Trizol reagent and PrimeScript RT reagent kit (Takara, Tokyo, Japan) according to manufacturer's instructions. Then diluted cDNA was mixed with TB Green™ Premix Ex Taq™ (Takara, Tokyo, Japan), forward and reverse primers and RNase free water to perform RT-qPCR. Osteogenic differentiation-related genes including ALP, Col I, Runx2 and OCN were evaluated, with GADPH used as housekeeping gene. Relative expression level for each gene (fold change) to that of blank control was calculated. Primer sequences used in this study were listed in Table 1.

2.5. Statistical analysis

All quantitative data are presented as mean ± SD and the quantitative experiments were carried out at least in triplicates. Differences among all groups were analyzed by one-way analysis of variance, and $^*p < 0.05$ was considered as statistically significant.

3. Results and discussion

3.1. Establishment of rat RME model and optimization of expanding parameters

In previous studies, RME models in rats were constructed with different expansion locations (anterior/posterior) and parameters (expansion force/time and retention time) [18–21]. Anterior maxillary expansion encounters less bone resistance by using incisors as anchorage, comparing to posterior maxillary expansion using molars. Previous studies used 30 g–100 g as expansion force and 5–7 days as

Table 1
Primer sequences used in real-time PCR analysis.

Gene	Primer Sequence	
	Forward	Reverse
GAPDH	ATGGCTACAGCAACAGGGT	TTATGGGGTCTGGGATGG
RUNX2	TCGGAAAGGGACGAGAG	TTCAAACGCATACCTGCAT
ALP	CCTACTTGTGTGGCGTGAA	GCAGGATGGACGTGACC
COL1	TGCAAGAACAGCGTAGCC	CAGCCATCCACAAGCGT
OCN	CGCCAGGGTGAAGAACTA	TACGCTGTGGAAGCCAA

expansion time, all of which could realize maxillary expansion [5,17,57], but might not represent severe MTD condition due to lack of standardized methods for model establishment, accurate parameter control, distance measurement and relapse rate calculation. So far, no systematic comparative study has been reported to determine the RME model parameters for an optimized simulation of severe MTD condition with insufficient bone regeneration.

In this study, anterior maxillary expansion was applied for rat RME model establishment, and a self-activated expander with precisely adjustable expanding force was designed (Fig. 1A). The expander was composed of a 2-mm helical spring and bilateral expanding arms with force-adjusting angles. In anterior expansion process, expander was

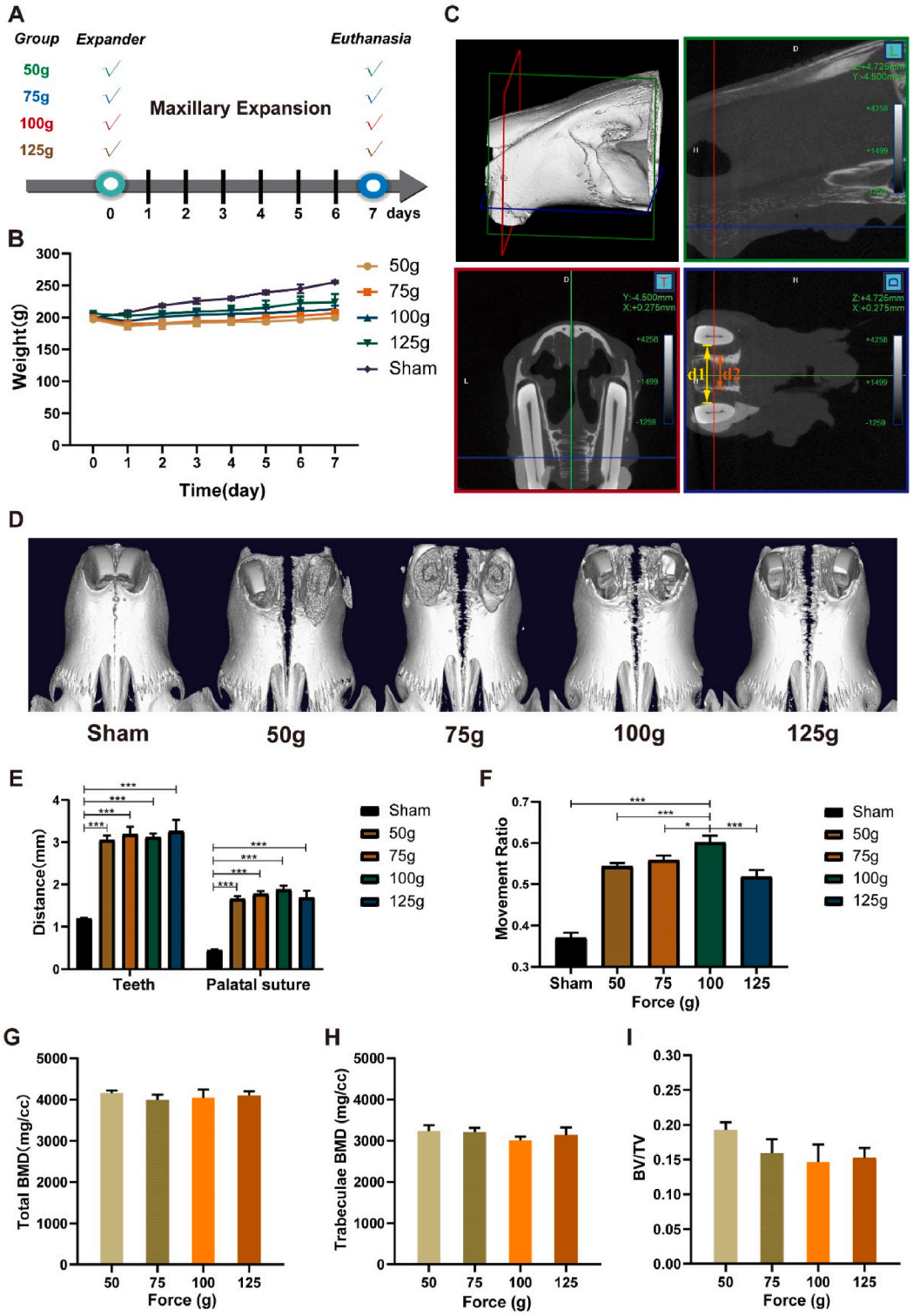

Fig. 2. Effect of different expansive forces on mid-palatal suture and teeth movement. (A) Time line of expansion. (B) Weight changes during 7-day expansion. (C) The sagittal, coronal and horizontal planes for measurement of the expanded distance between teeth (d1) and palatal suture (d2). (D) Three-dimensional micro-CT reconstruction images of the maxillae, (E) distances between mid-palatal suture and teeth and (F) relative movement of bone to teeth after 7-day expansion. Micro-CT quantification of (G) total BMD, (H) trabeculae BMD and (I) BV/TV (*$p < 0.05$, **$p < 0.01$, ***$p < 0.001$).

bound to incisors to exert indirect expanding force on maxillae through roots of incisors (Fig. 1B). After 7-day expansion, the gap between incisors was remarkably extended (Fig. 1C), then the helical spring was cemented by light curing resin to deactivate the expander and transform into retainer (Fig. 1D). Compared with previous studies [5,17,58,59], force-adjusting angles of the as-designed expander realized adjustable expanding force, more accurate expansive direction and better stability when transformed to retainer. Furthermore, the helical spring of expander is placed around the palatine papillae and tightly below the palatal mucosa to reduce discomfort to the rats, deemed as standardized position for expander.

In the previous literature, the expansion time of RME was mostly 7 days or 5 days. In our preliminary experiments, the maxillary expansion process during 14 days of continuous wearing of expander was observed. The outward movement of the incisors was noticeable within a week, while after that, the movement was hard to be observed by naked eyes. As measured via *in vivo* micro-CT imaging (Supplementary Fig. S1A), no significant difference in expanded skeletal distance was observed between expansion for 7 and 14 days, indicating a maximum expanded distance and resistance balance had been reached within 7 days. After resistance balance, though the distance was not further expanded, teeth distance was expanded compared to 7-day expansion, and the mid-palatal suture was filled with a certain amount of new bone by 14 days (Supplementary Figs. S1B–C). On this basis, the expanding time was set at 7 days for a rapid and maximum maxillary expansion. Extended expanding time did not further expand the suture and might increase risk of periodontitis.

For optimization of the model parameter, four expanding force

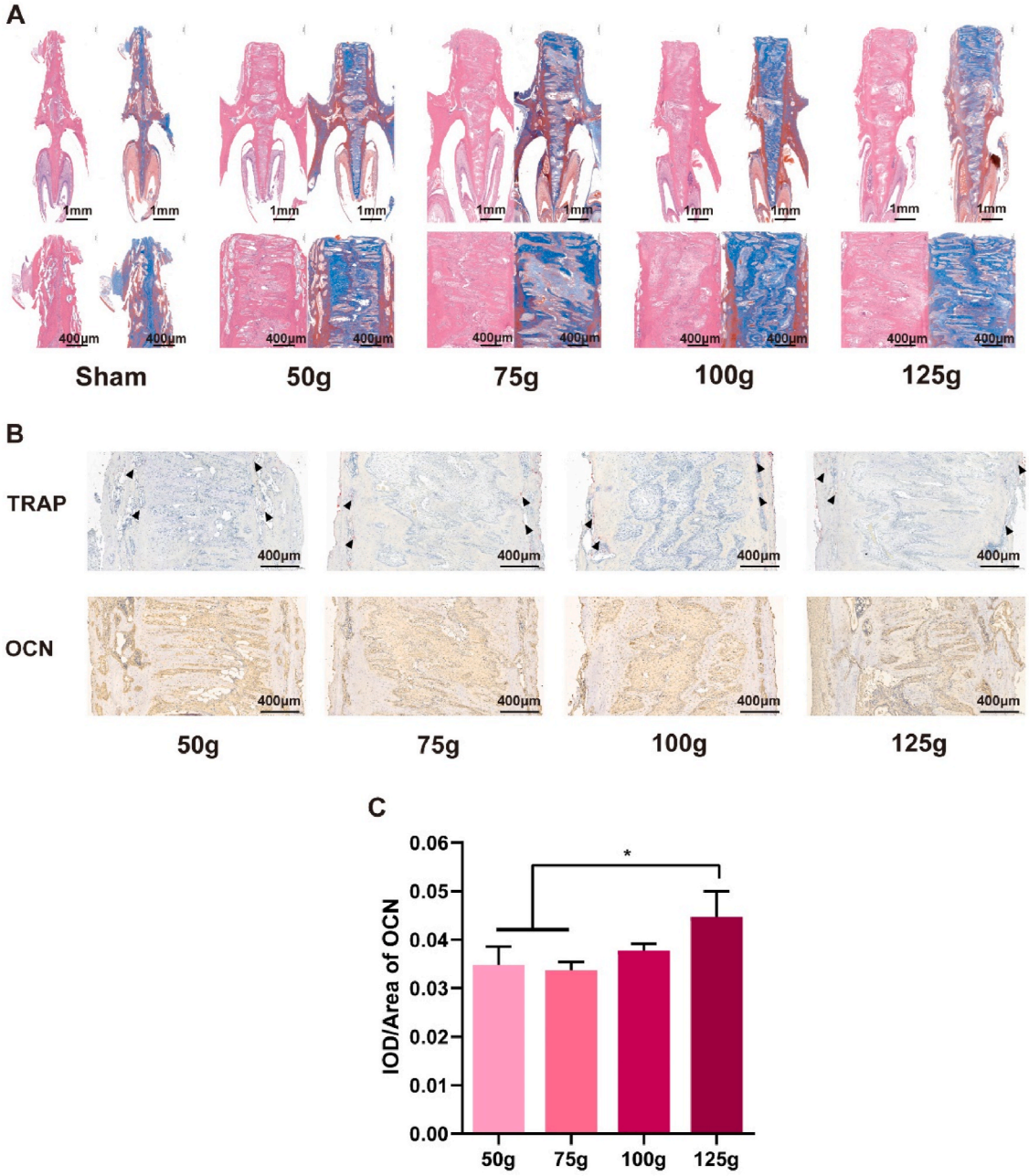

Fig. 3. Histological observations of the expanded mid-palatal suture after 7-day expansion by different force values. (A) HE and Masson's trichrome staining. (B) TRAP staining and immunohistochemical staining of osteocalcin (OCN). Black arrows indicate osteoclasts in mid-palatal suture. (C) IOD/Area density of OCN (*$p < 0.05$).

values were compared after 7 days of expansion (Fig. 2A). There was no significant periodontitis during expansion in all groups. In the expanding process, the weight gains of experimental rats were marginally lower than sham surgery group, though with no significant difference (Fig. 2B), implying that expansion slightly affects feeding. The relative position of incisor and maxilla changed under force: minor expansive force moved only the incisors and insufficient to expand the mid-palatal suture, while excessive force impaired the anchorage and aggravated the relative movement of suture and teeth [60–66]. Therefore, optimization of expansion force is critical to the establishment of RME model, yet no systematic study had been reported regarding the relationship between expansion force and incisor/maxillary suture expansion distance. As shown in Fig. 2C, distances between mid-palatal suture and incisors were measured by micro-CT. Compared with sham surgery group, the distances between mid-palatal suture and incisors in all experimental groups were significantly expanded, and distances between teeth were significantly larger than sutures (Fig. 2D). Though no significant difference of the teeth/suture distance were found among gradient expansive force values (Fig. 2E), the relative movement of suture and teeth in 100 g group was significantly higher than other groups (Fig. 2F), indicating 100 g force as an optimized value for RME model established by anterior expansion. Micro-CT quantification (Fig. 2G–I) indicated no significant differences among different force values in total bone mineral density (BMD), trabeculae BMD and bone volume/tissue volume (BV/TV).

In the rat RME model in this study, the incisors were expanded ~3 mm and the palatal suture ~1.8 mm (~0.26 mm/day) within 7 days. Considering the anatomical size differences between rats and human, the expansion speed of this model was much faster than clinical applications. Therefore, this animal model was considered to simulate extremely severe MTD including cleft lip and/or palate with high relapse rates due to insufficient bone regeneration, instead of mild MTD

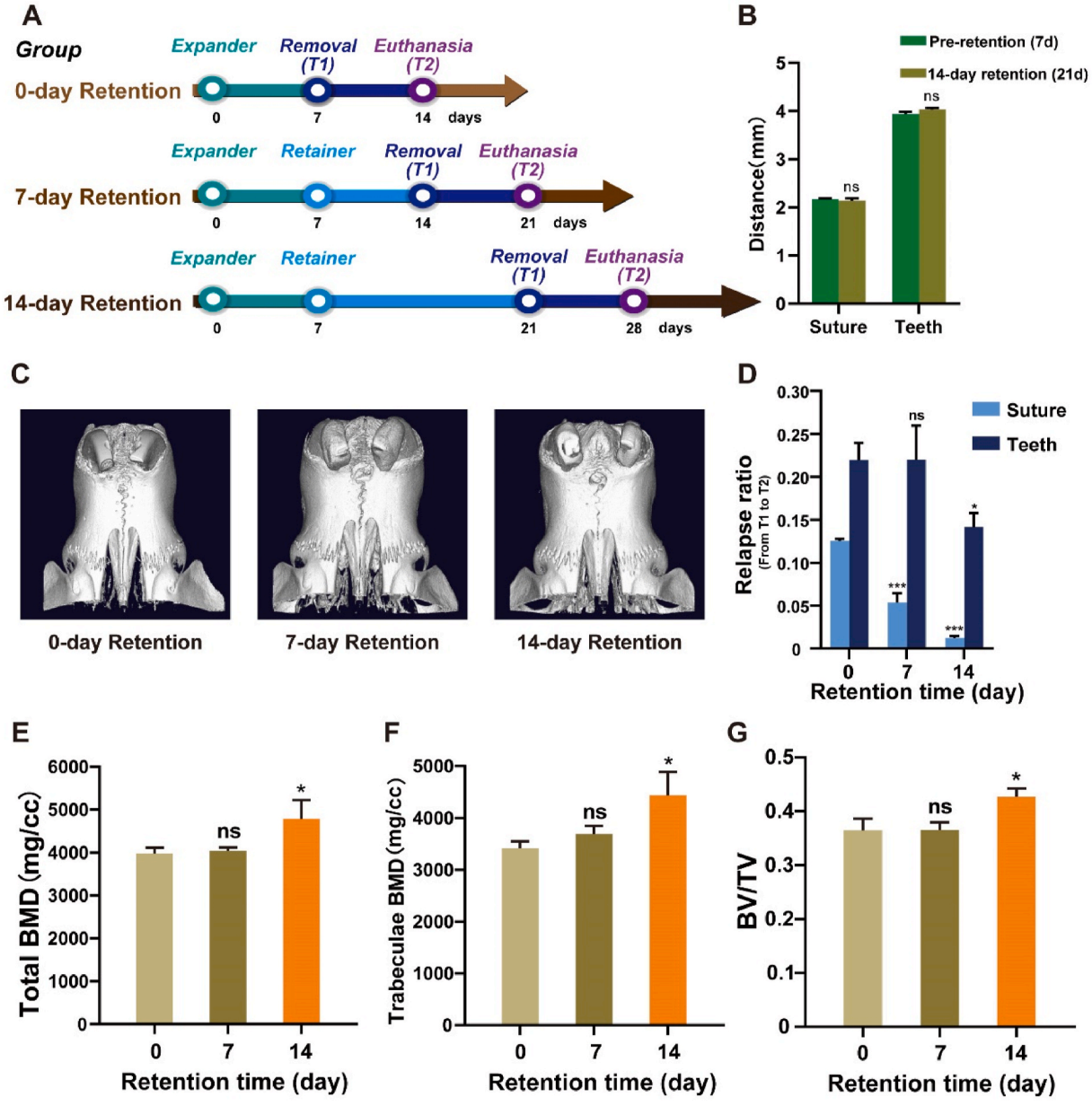

Fig. 4. Effects of retention on relapse and bone formation analyzed by micro-CT. (A) Time line of expansion and retention. (B) The skeletal and dental diastema measurement for the 14-day retention group rats before and after retention. (C) Representative comparison of micro-CT 3D reconstructed images for 0-day retention group, 7-day retention group and 14-day retention group. (D) The skeletal and dental relapse ratio for three groups. Quantitative analysis of (E) total BMD, (F) trabeculae BMD and (G) BV/TV (*$p < 0.05$, **$p < 0.01$, ***$p < 0.001$ and ns means no significance).

conditions and normal RME.

Histological observations exhibited that four expansive force values had significantly widened the mid-palatal suture to a V-shape, within the expanded sutures aligned new cartilage/bone tissue parallel to expansive direction, with gaps filled with fibrous tissue (Fig. 3A). TRAP staining showed a small number of osteoclasts distributed on the edge of the expanded mid-palatal suture in all groups, indicating that bone remodeling process had not yet begun after 7-day expansion (Fig. 3B). Immunohistochemical staining presented active expression of osteocalcin (OCN) within the expanded mid-palatal suture (Fig. 3B). The comparative analyses of OCN expression indicated no significant difference among all groups except 125 g group (Fig. 3C). These histological results indicated that expansive stress-initiated distraction osteogenesis based on endochondral osteogenesis process in mid-palatal suture.

Based on above results, 100 g expanding force was chosen as the optimized condition for rat RME model, and applied in the following experiments.

3.2. The relationship among retention time, osteogenesis and relapse ratio

To allow sufficient future osteogenesis and ensure no relapse post-expansion, it is common in clinic to adopt prolonged retention time, which is unnecessary and inapplicable in animal models. To determine a suitable post-expansion retention time for rat RME model, effects of different retention time (0/7/14 days) on relapse ratio and bone formation in mid-palatal suture were compared (Fig. 4A). During 14-day retention, no significant difference in suture/teeth distance were observed, indicating the effectiveness of the as-designed retainer (Fig. 4B). Micro-CT reconstruction of maxillae after removal of retainer for 7 days (Fig. 4C) showed that with prolonged retention time, both skeletal and dental relapse rate decreased (Fig. 4D), and bone formation (BV/TV) as well as bone mineralization density (BMD) increased within the expanded mid-palatal suture (Fig. 4E–G). The skeletal relapse rate was significantly reduced after 7/14-day retention, while dental relapse rate was not significantly influenced by 7-day retention and significantly reduced after 14-day retention (Fig. 4D). Quantitative analysis of micro-CT indicated that significantly increased bone formation only occurred in 14-day retention group (Fig. 4E–G). It was inferred that the as-established rat RME model could simulate the relationship among retention time, osteogenesis and relapse ratio in mid-palatal suture in clinic. In other words, sufficient osteogenesis was the key to reducing relapse ratio, which was achieved via prolonging retention time as a common clinical method.

Based on above results, retention time of 14 days was adopted for rat RME model as the shortest time that can significantly reduce relapse and improve osteogenesis within mid-palatal suture. Moreover, compared to dental relapse ratio which was commonly applied in previous studies [5], it was demonstrated that skeletal relapse ratio calculated by the distance of mid-palatal suture measured by micro-CT might be a more reliable indicator for relapse evaluation.

3.3. Fabrication and characterization of MBG/FG composite hydrogel

On account of the particularity of the injection site, properties of an ideal injectable osteogenic material included excellent biocompatibility, biodegradability, fluidity, sufficient mechanical strength, as well as osteoconduction and osteoinductivity to create a microenvironment for osteogenesis and mineralization. An injectable MBG/FG composite hydrogel was developed for *in situ* enhancement of bone formation within the mid-palatal suture. The FG hydrogel was synthesized via mixing fibrinogen and thrombin solution, while MBG particles were added in the fibrinogen solution at different ratios before mixture with thrombin (Scheme 1).

Mesoporous bioactive glass (MBG) was synthesized via typical evaporation-induced self-assembly (EISA) process with F127 as mesoporous template, then ground and sieved to obtain MBG particles (≤40 μm, ranging from nano-scale to micron-scale, Supplementary Fig. S2). Ordered and uniform mesoporous channels of MBG particles were observed by TEM (Fig. 5A). A capillary condensation step in N_2 adsorption-desorption analysis (Fig. 5B) demonstrated an ordered mesoporous structure and the mesopore size distribution showed a peak at 6.7 nm with high monodispersity (Fig. 5C), which provided the potential of drug delivery. The chemical composition of MBG was set at SiO_2: CaO: P_2O_5 = 85:15:5 for an optimal bioactivity as previously reported [46,47] and was confirmed by EDS (Fig. 5D). Wide-angle XRD spectrum (Fig. 5E) indicated a composition of amorphous silica, and typical diffraction peaks in the small-angle regime (Fig. 5F) could be indexed to the (110), (200), and (211) diffractions of a three-dimensional body centered cubic (Im3m) crystal lattice. The mesoporous structure of MBG could provide high surface area to interact with hydrogel matrix and could be used for drug delivery in further applications.

After incorporation of MBG particles, the fibrin glue (FG) hydrogel exhibited lower transparency. Injectability of the composite hydrogel decreased with MBG particle ratio, and fibrinogen solution with over 5 wt% of MBG became uninjectable. Hence the properties of composite MBG/FG hydrogels (Fig. 5G) with MBG particle content ranging from 0.5% to 4% were investigated. The surface microstructures observed by SEM showed that under a 200× magnification, surface roughness of the hydrogel increased with MBG ratio: pure FG hydrogel exhibited a smooth surface, while escalating granular structures were observed with the increasing of MBG ratio. Whereas under a higher magnification (1000 ×), pure FG hydrogel presented a relatively loose fibrous structure, while the surfaces of MBG/FG composite hydrogels were more compact. EDS element mappings of P, Si and Ca in FG and FG/MBG composite hydrogels were shown in Fig. 5H. The signal intensities of P, Si and Ca increased with MBG contents and were evenly distributed in the hydrogels, indicating homogeneous composition.

Appearance of FG and MBG/FG composite hydrogels are shown in Fig. 6A, and it can be seen that with higher ratio of MBG particles incorporation, the hydrogel exhibited lower transparency and more maldistribution. The rapid reaction of fibrinogen cross-linking by thrombin was completed within seconds after mixture and presented in Supplementary Video. To be noted, gelation of MBG/FG was significantly faster than pure FG, which was attributed to the existence of Ca^{2+} in MBG as a typical coagulation factor.

Supplementary video related to this article can be found at https://doi.org/10.1016/j.bioactmat.2022.03.001.

Mechanical test results showed that the incorporation of MBG particles significantly enhanced the compressive strength of the composite hydrogel compared to pure FG, and there were no significant differences among the groups with ≥1% MBG (Fig. 6B and C). As shown in the degradation profiles (Fig. 6D), pure FG hydrogel exhibited a rapid degradation and completely degraded in 6 days; the degradation rate slowed down after incorporation of 0.5% MBG, and 0.5%MBG/FG hydrogel completely degraded at 14 days; hydrogels with ≥1% MBG exhibited a similar slow degradation rate and only degraded about 20% at 14 days. Based on the above results and the known mechanism of fibrin formation [34,42], it is inferred that Ca^{2+} ions in MBG particles, also recognized as a coagulation factor, promoted fibrin crosslinking and formed more crosslinking sites, hence significantly enhanced mechanical strength and hydrogel stability. The similar mechanical and degradation properties of MBG/FG composite hydrogels with ≥1% MBG could be attributed to the upper limit of FG crosslinking degree. The degradation of MBG material was mainly through ion release [67,68]. Ionic dissolution curves (Fig. 6E and F) showed that all groups of composite hydrogels released Ca^{2+} and SiO_4^{4-} at a constant rate. The dissolution rate of Ca^{2+} was faster than SiO_4^{4-}, despite that the content of Si was higher than Ca in material composition. Ca^{2+} ions in 0.5%MBG/FG composite hydrogel were completely dissolved after 14 days, which was consistent with the overall degradation of the composite hydrogel, while

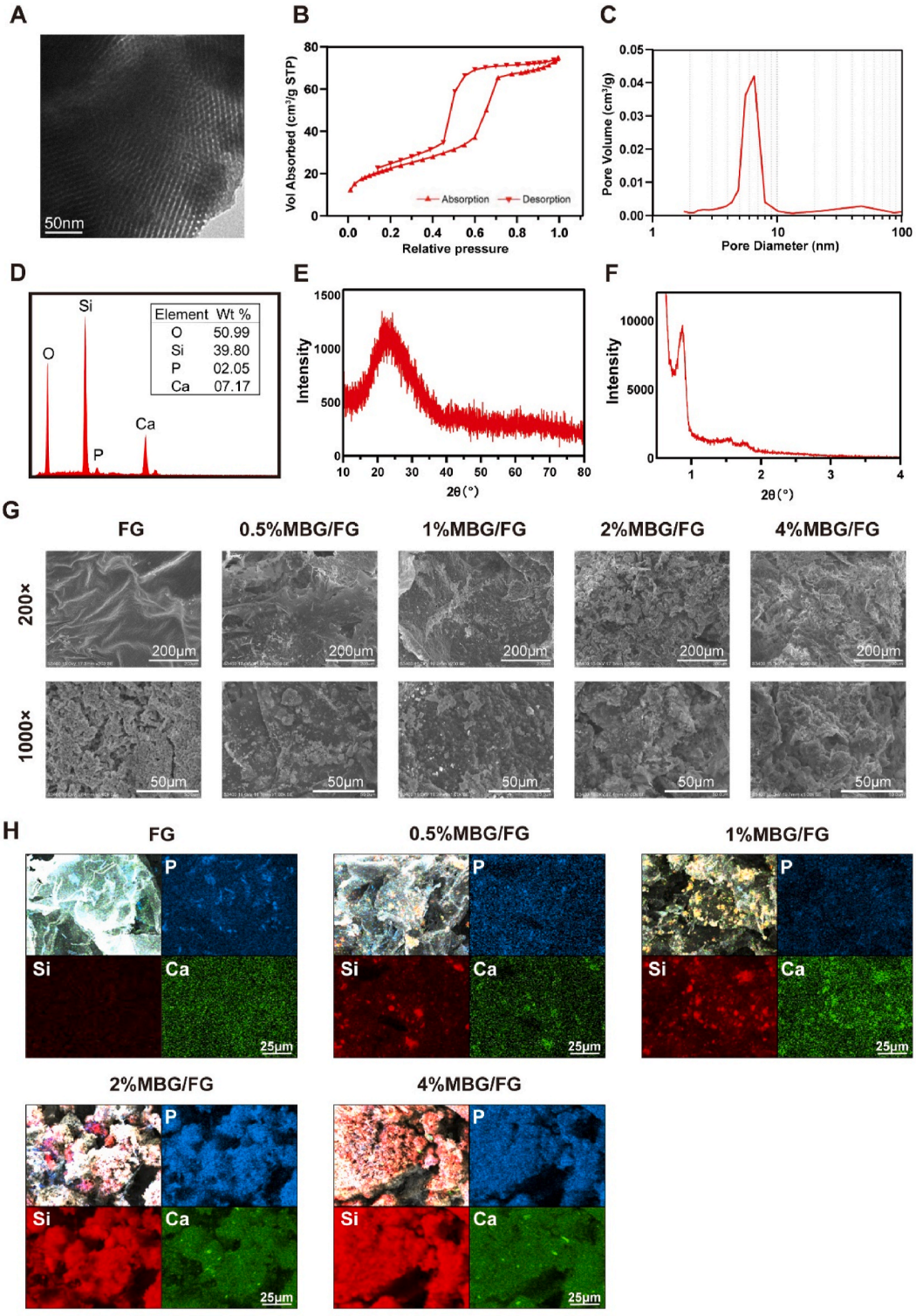

Fig. 5. Characterizations of MBG particles, FG hydrogel and MBG/FG composite hydrogels. (A) Mesoporous structure observed by TEM, (B) N_2 adsorption-desorption isotherm and (C) the corresponding pore size distribution, (D) EDS spectrum, (E) Wide-angle XRD and (F) small-angle XRD of MBG particles. (G) Surface morphology of FG and MBG/FG composite hydrogels observed by SEM. (H) Element mapping including P, Si and Ca of FG and MBG/FG composite hydrogels detected by EDS.

SiO_4^{4-} ions dissolved only approximately 35% at day 14, indicating that large amount of MBG particles remained undegraded when 0.5% MBG/FG hydrogel matrix completely degraded. In contrast, MBG dissolution and FG degradation were more synchronous in 1%MBG/FG, 2%MBG/FG and 4%MBG/FG hydrogels. Stable release of Ca^{2+} and SiO_4^{4-} from MBG/FG composite hydrogel could regulate cell differentiation and promote bone formation [69–72].

In this study, thrombin was applied to coagulate fibrinogen solution. Calcium ions, namely coagulation factor IV, were rich in MBG particles. Together with thrombin, they have synergetic effect on the crosslinking of MBG/FG composite hydrogels. The mechanical enhancement of MBG/FG hydrogel might be the result of particle reinforcement and

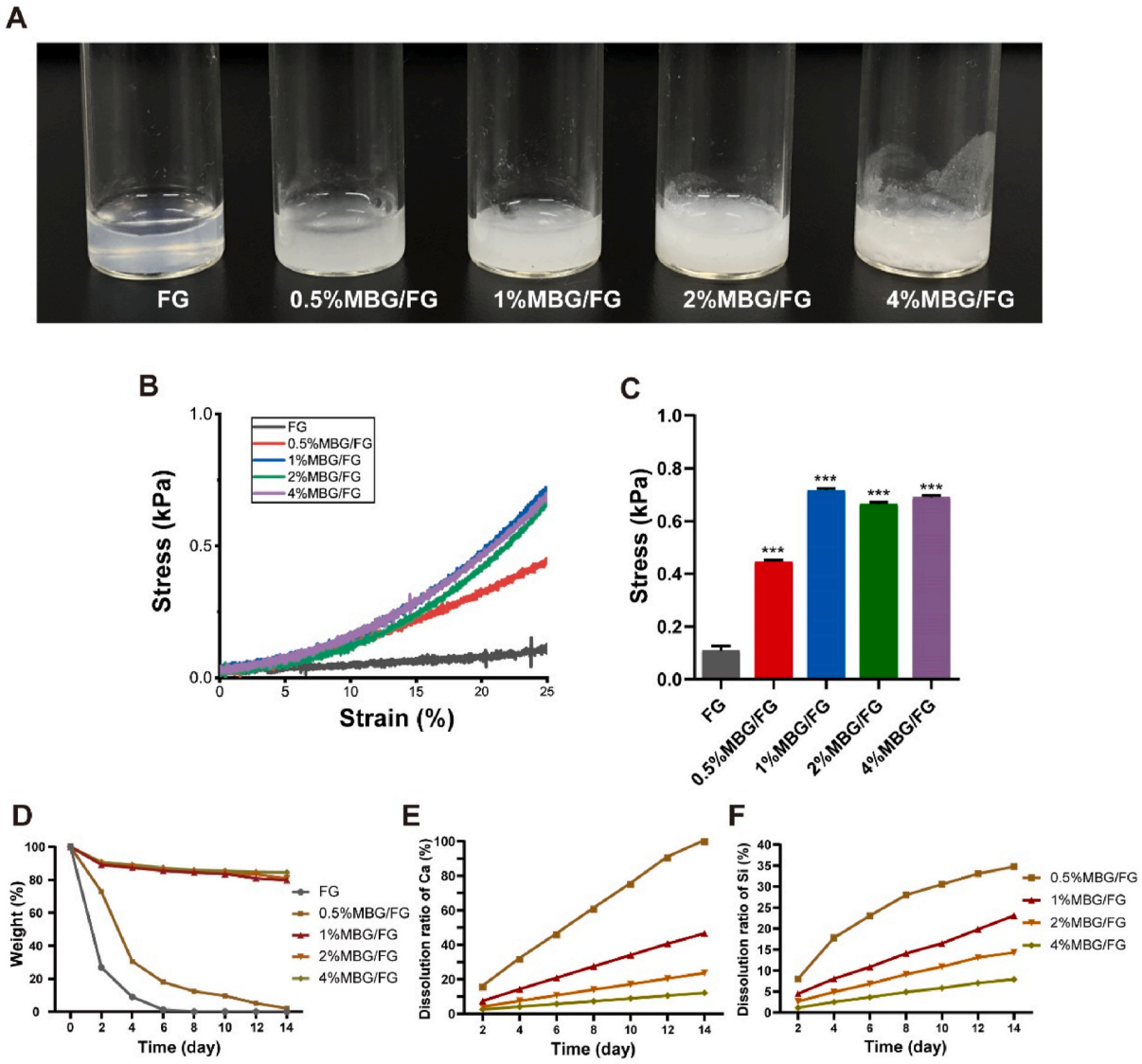

Fig. 6. Material properties of MBG/FG composite hydrogels. (A) The visual form of FG and MBG/FG composite hydrogels. (B) Compression stress-strain curves and (C) compressive strength of FG and MBG/FG composite hydrogels at 25% strain ratio. (D) In vitro degradation curves. Ion dissolution of (E) Ca and (F) Si from MBG/FG composite hydrogels.

higher crosslinking degree induced by Ca^{2+}, and the slower degradation also suggested a crosslinking degree.

3.4. *In vitro cytocompatibility and osteoinductivity of MBG/FG hydrogel*

The FG and MBG/FG composite hydrogels were co-cultured with rat BMSCs (rBMSCs) for evaluation of cytotoxicity, cell adhesion and osteoinductivity. Results of CCK-8 assay and cytoskeleton staining demonstrated excellent cytocompatibility and cell adhesion properties of all FG and MBG/FG composite hydrogels with no significant difference among the groups (Fig. 7A and B).

Osteoinductivity of bioactive glass and fibrin glue have both been acknowledged in previous studies [56,71,73]. Based on these research backgrounds, this paper had chosen MBG and FG as hydrogel components for *in vivo* bone regenerative enhancement. It is commonly acknowledged that MBG induces osteogenesis via dissolution of calcium and phosphorus ions. Herein, osteoinductivity of FG and MBG/FG composite hydrogels were evaluated by ALP, mineralization staining and osteogenic related gene expression. Results of ALP staining and ALP activity quantification (Fig. 8A and B) indicated a limited osteoinductivity of pure FG hydrogel with no significant difference compared to control group. Incorporation of MBG particles significantly increased the ALP activity of the composite hydrogel, but with no significant difference among different MBG contents. As above-mentioned, the calcium release rate of the MBG/FG hydrogels with different MBG contents were basically identical (Fig. 6E), indicating that the incorporated MBG particles promoted osteogenic differentiation via ion dissolution. Alizarin red staining also confirmed that MBG/FG composite hydrogel enhanced mineralization of rBMSC at a later stage, with 1% MBG/FG composite hydrogel exhibiting the highest mineral deposition (Fig. 8C).

Taken together, considering the material properties (injectability, mechanical, biodegradability) and biological properties (cytocompatibility, osteoinductivity) of the composite hydrogel, 1%MBG/FG composite hydrogel was selected for further experimental study and palatal suture injection in rat RME model. QRT-PCR results (Fig. 8D–G) showed that after 7 days of co-culture, 1%MBG/FG composite hydrogel significantly upregulated the expression of early osteogenic markers Runx2 and ALP to a similar level of pure MBG, while pure FG hydrogel exerted no significant influence on Runx2 and ALP expression. Whilst pure FG

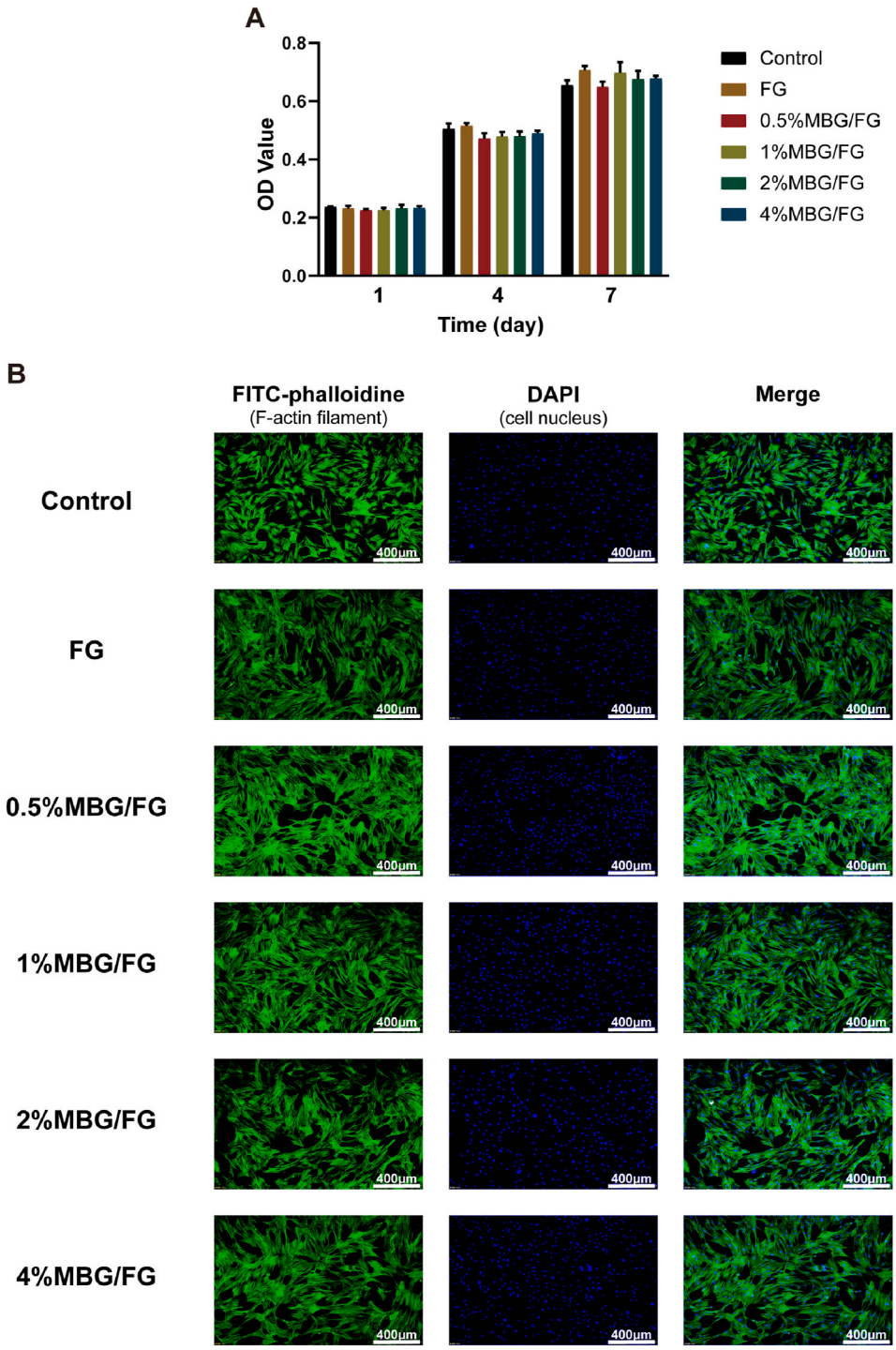

Fig. 7. Cytocompatibility and cell adhesion of FG and MBG/FG composite hydrogels. (A) CCK-8 assay. (B) Cytoskeleton staining of rBMSCs co-cultured with the hydrogels for 24 h.

upregulated Col-1 expression to a highest level, and 1%MBG/FG composite hydrogel exhibited highest expression of late osteogenic marker OCN.

It is reported that fibrous structure of FG could promote cell adhesion and facilitated osteoblasts differentiation via integrin-mediated pathway [34]. The release of calcium ion and phosphate ion from MBG induced osteogenic differentiation [74–76] and silicate ion promoted angiogenesis [77–79] and inhibited inflammation [80–82]. Therefore, combining the merit of FG and MBG, 1%MBG/FG was demonstrated to be a promising injectable composite hydrogel that promoted osteogenesis and mineralization.

3.5. Relapse reduction and osteogenesis enhancement by injection of MBG/FG hydrogel

As a general treatment that effectively reduce the relapse of RME, the essence of long-term retainer wearing is to maintain a state of constant stress that allows bone ingrowth. *In situ* injection of biomaterials can be used as a minimally invasive treatment to accelerate the bone formation process [30–33]. In this study, with retainer wearing and hydrogel injection as two variables, four groups of post-RME treatment were set for evaluation of relapse reduction and bone formation (Fig. 9A). *In situ* injection of MBG/FG composite hydrogel into the expanded mid-palatal

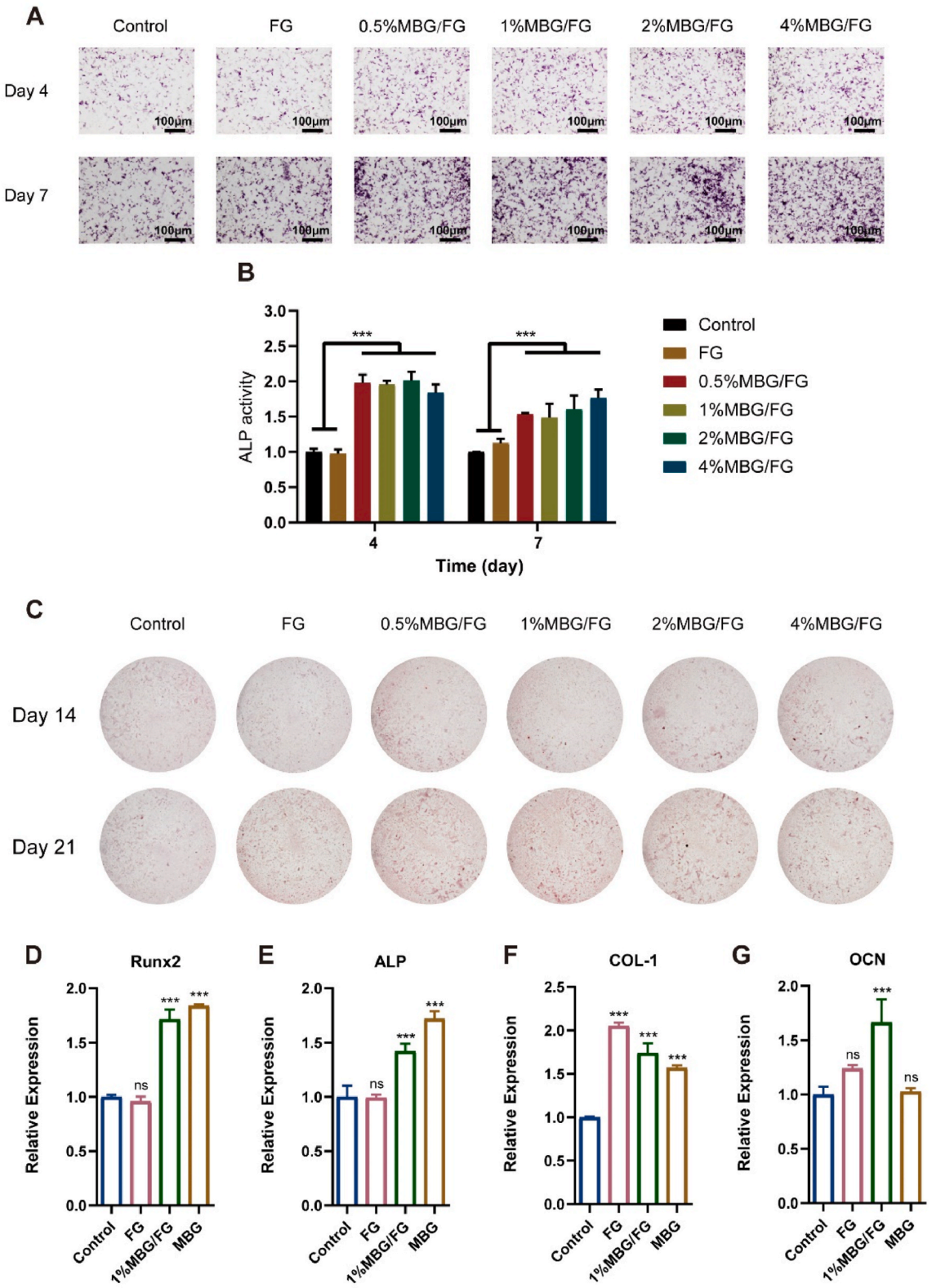

Fig. 8. In vitro evaluation of the osteoinductivity of FG and MBG/FG hydrogels. (A) ALP staining, (B) ALP activity and (C) Alizarin red S staining. Expression of osteogenic-related genes: (D) Runx2, (E) ALP, (F) Col-1 and (G) OCN via RT-qPCR (***$p < 0.001$).

suture was schematically illustrated in Fig. 9B. Similar to clinical phenomena, groups without retainers after expansion (Ctrl and I) showed certain relapse rates, while retainer wearing efficiently prevented relapse (R and R+I groups) (Fig. 9C). Under the retainerless condition, the relapse rate of group I was significantly lower than Ctrl, indicating that hydrogel injection alone could reduce relapse rate to some extent. Micro-CT three-dimensional reconstruction (Fig. 9D) presented better-healed surfaces of mid-palatal suture in I and R+I than both Ctrl and R groups, and quantitative analyses of BV/TV, total BMD and trabecular bone BMD (Fig. 9E–G), indicating that injection of 1%

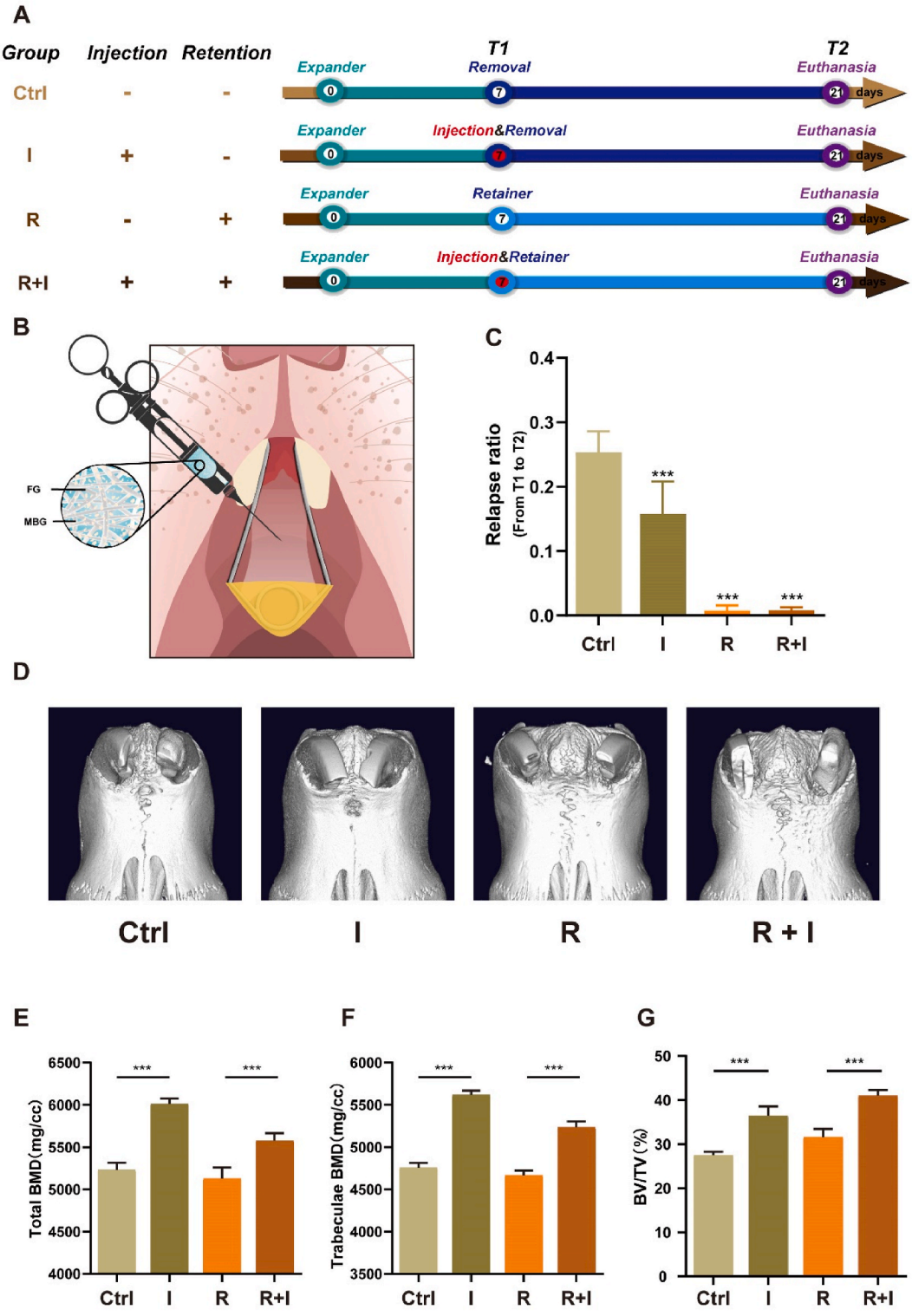

Fig. 9. Influence of injections and/or retention on osteogenesis in the expanded mid-palatal suture by micro-CT. (A) Group settings and time line of treatment. (B) Schematic illustration for submucosal injection of 1%MBG/FG composite hydrogels into mid-palatal suture. (C) Skeletal relapse ratio. (D) Three-dimensional micro-CT reconstruction images of the maxillae. Micro-CT quantification of (E) total BMD, (F) trabeculae BMD and (G) BV/TV (***$p < 0.001$).

MBG/FG composite hydrogel significantly enhanced osteogenesis and mineralization within the mid-palatal suture.

Histological observation via HE and Masson's trichrome staining were shown in Fig. 10A. Without retaining, both Ctrl and I groups presented obvious non-osseous gaps in the middle of suture, and in comparison, group I showed a relatively narrower non-osseous gap and higher bone maturity within the suture (stained red in Masson's trichrome staining). After retaining, the expanded mid-palatal sutures of R and R+I were wider with negligible non-osseous gap and more trabecular bone. R+I group showed a highest amount of trabecular bone among all groups. The histological results indicated no excessive inflammation or fibrosis in the expanded suture. As a biogenetic

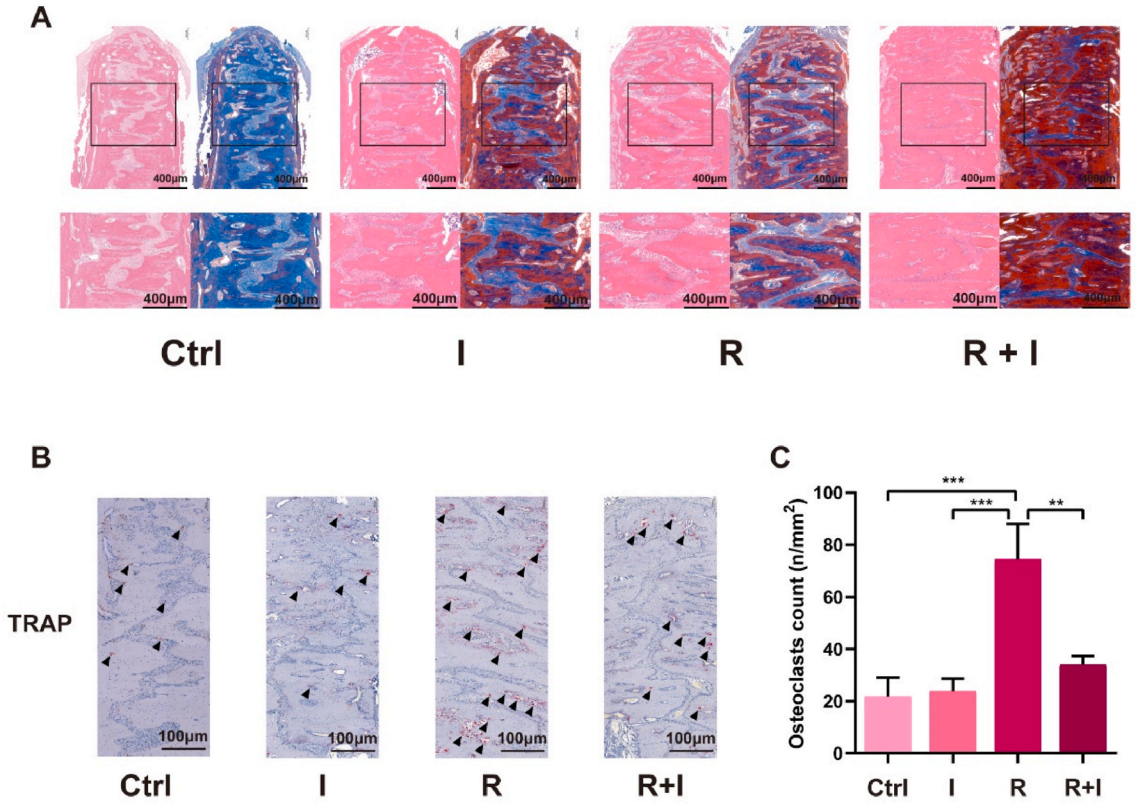

Fig. 10. Influence of injections and/or retention on osteogenesis in the expanded mid-palatal suture by histological staining. (A) HE and Masson's trichrome staining. (B) TRAP staining and (C) its corresponding quantification (**p < 0.01, ***p < 0.001). Black arrows indicate osteoclasts in mid-palatal suture.

derivative, FG can be completely absorbed during wound healing without foreign body reaction or extensive fibrosis [83]. Earlier literature has shown that FG diminishes epidural scar formation [84]. In addition, minimizing tissue injury and good hemostasis have been proven most effective in preventing fibrosis [85]. It is reported that bioglass ionic products control inflammation and promote regeneration by regulating M2 polarization of macrophages [86]. Bioglass has also been reported to stimulate fibroblasts to secrete factors that promote vascularization at the wound site [87]. Another study showed that MBG is non-toxic and non-inflammagenic for immunocytes [88]. Therefore, on the bases of previous literature and as proven by the histological results here, the minimally invasive injection of MBG/FG composite hydrogel adopted in this study did not cause excessive inflammation or fibrosis. Histologic sections indicated that 1%MBG/FG composite hydrogels had been completely degraded in mid-palatal suture after 14 days of retention. Though the hydrogels exhibited a relatively slow degradation rate and only degraded about 20% at 14 days *in vitro*, material degradation *in vivo* often accelerated due to cellular or biochemical reactions. It is reported that FG was enzymatically catabolized by plasmin *in vivo* [38], resulting in complete degradation of hydrogel *in vivo* in 14 days.

Since the expansion of mid-palatal suture is a process of bone remodeling balanced by osteoblasts and osteoclasts, number and distribution of osteoclasts were further analyzed by TRAP staining to evaluate the state of bone remodeling in different groups (Fig. 10B). The red stained osteoclasts were distributed mostly at the edge of bone trabeculae and minorly in the non-osseous fibrous tissue. Quantitative analysis (Fig. 10C) indicated fewer osteoclasts in both Ctrl and I groups, suggesting that the process of bone remodeling was completed and relatively inactive after 14 retainerless days. R group showed the highest number of osteoclasts, verifying a more active remodeling by osteoclast under constant retention stress; while the number of osteoclasts in R+I was significantly reduced, indicating that injection of 1%MBG/FG composite hydrogel could accelerate bone remodeling process and inhibit osteoclast differentiation, thus promoting bone formation in mid-palatal suture. Immunohistochemical staining (Fig. 11A) and quantitative analyses showed that OCN and CD31, markers of early osteogenesis, were highly expressed in the palatal suture of group I and R, while in R+I were relatively low (Fig. 11B and C). Since R+I group showed the highest amount of trabecular bone, low expression of early osteogenic markers was considered as the sign of completion of early osteogenesis in group R+I at the same time point. Previous studies used the relative value of RANKL and OPG to reflect the dynamic balance state of osteoclast and osteogenesis [18,89–91]: higher relative value of RANKL/OPG suggested dominance of osteoclastogenesis, while lower suggested osteogenesis. Group R showed the highest expression of RANKL (Fig. 11D), which was similar to the trend of TRAP staining; while OPG expression was highest in R+I (Fig. 11E). By comparing the relative value of RANKL/OPG (Fig. 11F), an obvious trend could be observed that injection groups (I and R+I) were significantly low than the uninjected groups (Ctrl and R), indicating that injection of 1% MBG/FG composite hydrogel significantly promoted the bone formation within the mid-palatal suture, and benefited the balance of bone remodeling towards osteogenesis.

Osteogenesis in the palatal suture was further observed via undecalcified VG staining and sequential fluorescence labeling. As shown in undecalcified VG staining images (Fig. 12A), groups without retention (Ctrl and I) exhibited nondirectionally oriented bone trabeculae compared to the retention groups (R and R+I). The number of new bone trabeculae in the injection groups (I and R+I) were significantly increased compared with the groups without injection (Ctrl and R). Sequential fluorescent label was applied to quantify the amount and rate of mineralization during bone regeneration. As shown in Fig. 12B, fluorescent images also exhibited the directional alignment oriented by retention treatment. Ctrl group exhibited the least fluorescent bands, which were significantly increased by hydrogel injection and/or

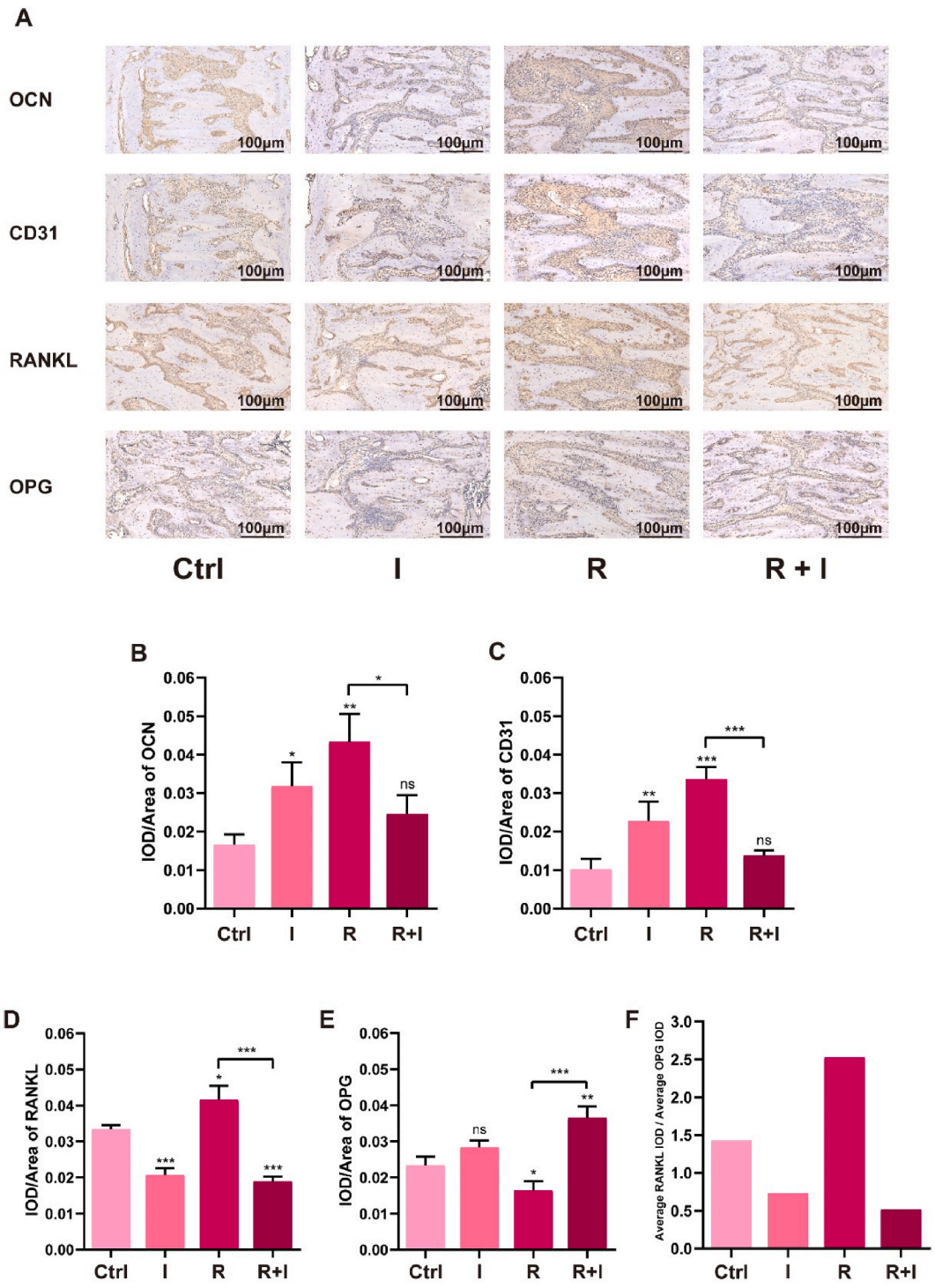

Fig. 11. Immunohistochemical staining and quantitive analyses. (A) IHC staining of OCN, CD31, RANKL and OPG expression. IOD/Area density of (B) OCN, (C) CD31, (D) RANKL and (E) OPG. (F) The relative value of average RANKL IOD to average OPG IOD (*$p < 0.05$, **$p < 0.01$, ***$p < 0.001$ and ns means no significance). IOD: integrated optical density.

retention. Green bands represented the calcium deposition at the initial stage, and red represented deposition after 7-day retention. Quantitative analysis of MAR and relative fluorescence area showed that injection groups I and R+I were significantly increased compared with Ctrl and R groups, indicating that injection of 1%MBG/FG composite hydrogel significantly improved the mineral deposition rate and new bone formation in the palatal suture area.

The results of animal experiments demonstrated the excellent *in vivo* osteogenic property of the as-developed 1%MBG/FG composite hydrogel, with good injectability that could meet the requirements of clinical maxillofacial bone repair. In addition, the standardized rat RME model established in this study proved that combination of retainer and injectable biomaterial after RME was a better way to avoid relapse and promote new bone formation.

4. Conclusion

This study had established a standardized rat RME model with

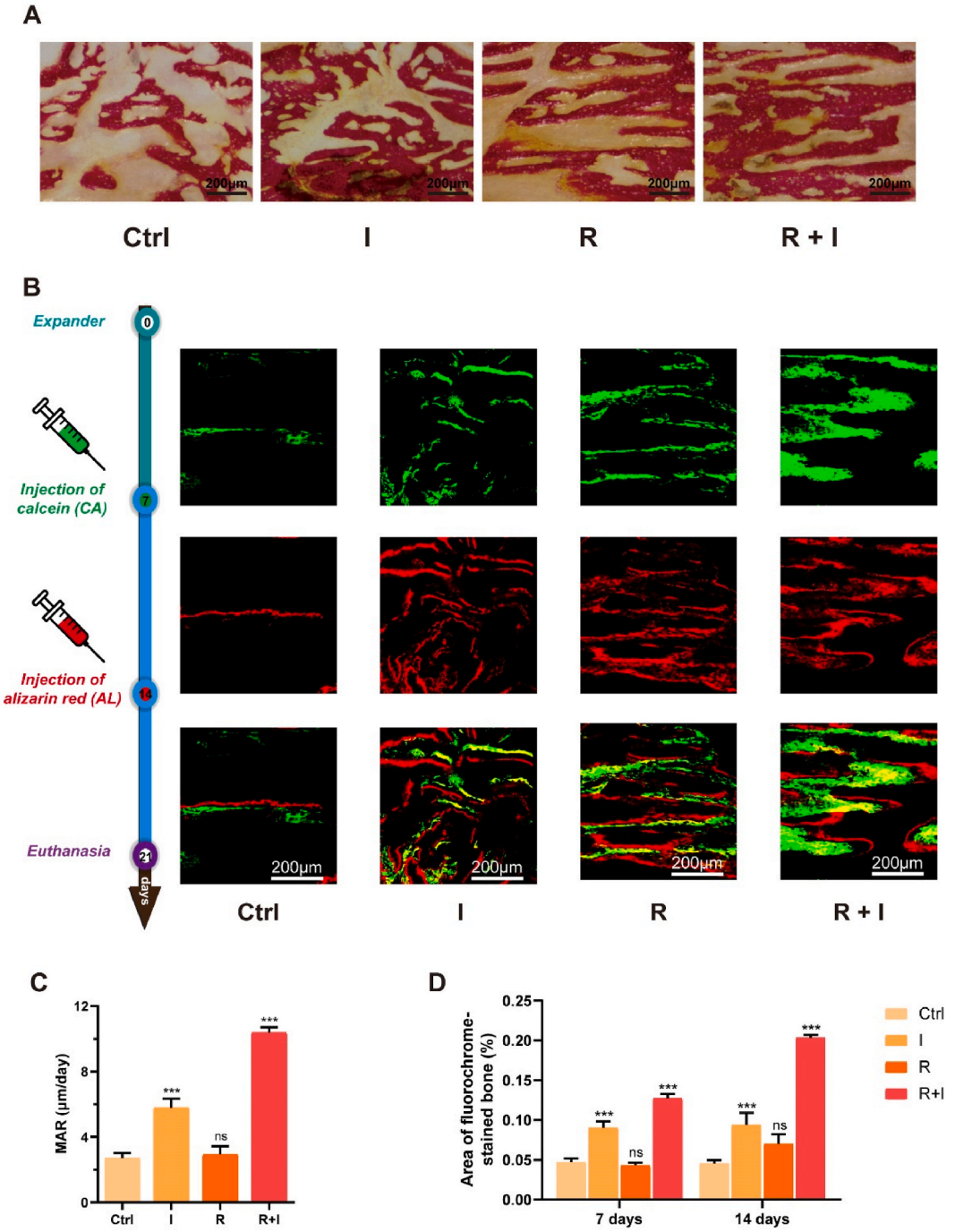

Fig. 12. The observation of osteogenesis and mineralization. (A) Histological evaluation of undecalcified mid-palatal suture with VG staining. (B) Fluorescence observation by confocal laser scanning microscopy (CLSM). The corresponding quantification of (C) mineral apposition rate (MAR) and (D) stained bone area (***$p < 0.001$ and ns means no significance).

optimized mechanical parameters and modified retainer design to simulate severe MTD conditions with insufficient bone regeneration. Via the standardized rat RME model, injectable MBG/FG composite hydrogels were designed for osteogenic enhancement and relapse reduction in RME. An optimized component of 1%MBG/FG was demonstrated with highest mechanical strength, matched degradation rate and ion dissolution, excellent *in vitro* biocompatibility and osteoinductivity. *In vivo* osteogenic efficiency of 1%MBG/FG composite hydrogel was further verified in the established rat RME model, exhibiting outstanding osteogenesis, mineralization and angiogenesis performance while inhibiting osteoclastogenesis in the expanded mid-palatal suture. Combinatory treatment of retention and *in situ* material injection after RME was proven as an improved strategy for relapse reduction and osteogenesis enhancement. The standardized rat RME model as well as modified retainer design reported in this article might provide new insight on the research of other craniomaxillofacial deformities. The as-designed MBG/FG composite hydrogel was prospected as a promising injectable biomaterial for clinical translation with FDA-approved components, which could be extended to other craniomaxillofacial and orthopedic DO applications and arouse broader interests of researchers.

CRediT authorship contribution statement

Hanjiang Zhao: Conceptualization, Methodology, Investigation, Visualization, Writing – original draft. **Xiangyu Wang:** Conceptualization, Methodology. **Anting Jin:** Conceptualization, Methodology. **Minjiao Wang:** Methodology, Investigation. **Zeying Wang:** Methodology. **Xingtai Huang:** Methodology. **Jiewen Dai:** Resources, Funding acquisition. **Xudong Wang:** Supervision, Project administration, Funding acquisition. **Dan Lin:** Conceptualization, Methodology, Investigation, Visualization, Writing – review & editing. **Steve GF. Shen:** Supervision, Project administration, Funding acquisition.

Declaration of interests

The authors declare that they have no known competing financial interests or personal relationships that could have appeared to influence the work reported in this paper.

Acknowledgements

The authors gratefully acknowledge the support of the National Natural Science Foundation of China (No. 81970973, No. 81771036, No. 82071097, No. 82071096), China Postdoctoral Science Foundation (2020T130422), Shanghai Sailing Program (19YF1425500, 19YF1426500).

Appendix A. Supplementary data

Supplementary data to this article can be found online at https://doi.org/10.1016/j.bioactmat.2022.03.001.

References

[1] M. Zandi, A. Miresmaeili, A. Heidari, Short-term skeletal and dental changes following bone-borne versus tooth-borne surgically assisted rapid maxillary expansion: a randomized clinical trial study, J. Cranio-Maxillo-Fac. Surg. 42 (7) (2014) 1190–1195.
[2] C. Carlson, J. Sung, R.W. McComb, A.W. Machado, W. Moon, Microimplant-assisted rapid palatal expansion appliance to orthopedically correct transverse maxillary deficiency in an adult, Am. J. Orthod. Dentofacial Orthop. 149 (5) (2016) 716–728.
[3] N.M.F. Neyt, M.Y. Mommaerts, J.V.S. Abeloos, C.A.S. De Clercq, L.F. Neyt, Problems, obstacles and complications with transpalatal distraction in non-congenital deformities, J. Cranio-Maxillo-Fac. Surg. 30 (3) (2002) 139–143.
[4] B.A. Vandersea, A.T. Ruvo, D.E. Frost, Maxillary transverse deficiency - surgical alternatives to management, Oral Maxillofac. Surg. Clin. 19 (3) (2007).
[5] C. Hong, D. Song, D.K. Lee, L. Lin, H.C. Pan, D. Lee, P. Deng, Z. Liu, D. Hadaya, H. L. Lee, A. Mohammad, X. Zhang, M. Lee, C.Y. Wang, D. Ho, Reducing posttreatment relapse in cleft lip palatal expansion using an injectable estrogen-nanodiamond hydrogel, Proc. Natl. Acad. Sci. U. S. A. 114 (35) (2017) E7218–E7225.
[6] M. Khosravi, A. Ugolini, A. Miresmaeili, H. Mirzaei, V. Shahidi-Zandi, S. Soheilifar, M. Karami, M. Mahmoudzadeh, Tooth-borne versus bone-borne rapid maxillary expansion for transverse maxillary deficiency: a systematic review, Int. Orthod. 17 (3) (2019) 425–436.
[7] F. Fatima, W. Jeelani, M.J.D. Ahmed, Current trends in craniofacial distraction: a literature review 57 (4) (2020) 441–448.
[8] M.C.D. Andrucioli, M.A.N. Matsumoto, Transverse maxillary deficiency: treatment alternatives in face of early skeletal maturation, Dental Press J. Orthod. 25 (1) (2020) 70–79.
[9] A.C. Aloise, M.D. Pereira, C.T. Hino, A.G. Filho, L.M. Ferreira, Stability of the transverse dimension of the maxilla after surgically assisted rapid expansion, J. Craniofac. Surg. 18 (4) (2007) 860–865.
[10] N.M. Neyt, M.Y. Mommaerts, J.V. Abeloos, C.A. De Clercq, L.F. Neyt, Problems, obstacles and complications with transpalatal distraction in non-congenital deformities, J. Cranio-Maxillo-Fac. Surg. 30 (3) (2002) 139–143.
[11] B.K. Hall, Cellular differentiation in skeletal tissues, Biol. Rev. Camb. Phil. Soc. 45 (4) (1970) 455–484.
[12] I. Takahashi, I. Mizoguchi, M. Nakamura, Y. Sasano, S. Saitoh, M. Kagayama, H. Mitani, Effects of expansive force on the differentiation of midpalatal suture cartilage in rats, Bone 18 (4) (1996) 341–348.
[13] E.T. Kobayashi, F. Hashimoto, Y. Kobayashi, E. Sakai, Y. Miyazaki, T. Kamiya, K. Kobayashi, Y. Kato, H. Sakai, Force-induced rapid changes in cell fate at midpalatal suture cartilage of growing rats, J. Dent. Res. 78 (9) (1999) 1495–1504.
[14] M. Sawada, N. Shimizu, Stimulation of bone formation in the expanding mid-palatal suture by transforming growth factor-beta 1 in the rat, Eur. J. Orthod. 18 (2) (1996) 169–179.
[15] B. Hou, E. Kolpakova-Hart, N. Fukai, K. Wu, B.R. Olsen, The polycystic kidney disease 1 (Pkd1) gene is required for the responses of osteochondroprogenitor cells to midpalatal suture expansion in mice, Bone 44 (6) (2009) 1121–1133.
[16] J. Chen, J. Zhou, F. Li, J. Sun, G. Li, S. Zou, Q. Ye, Expression of MMP-2 and TIMP-1 during rapid maxillary expansion in rats, Arch. Oral Biol. 76 (2017) 30–35.
[17] B.A. Altan, I.M. Kara, R. Nalcaci, F. Ozan, S.M. Erdogan, M.M. Ozkut, S. Inan, Systemic propolis stimulates new bone formation at the expanded suture: a histomorphometric study, Angle Orthod. 83 (2) (2013) 286–291.
[18] J. Yi, L. Mei, X. Li, W. Zheng, Y. Li, Z. Zhao, Effects of continuous and intermittent parathyroid hormone administration on midpalatal suture expansion in rats, Arch. Oral Biol. 99 (2019) 161–168.
[19] A. Utreja, C. Bain, B. Turek, R. Holland, R. AlRasheed, P. Sorkhdini, W.E. Roberts, Maxillary expansion in an animal model with light, continuous force, Angle Orthod. 88 (3) (2018) 306–313.
[20] Y. Cheng, J. Sun, Z. Zhou, J. Pan, S. Zou, J. Chen, Effects of lactoferrin on bone resorption of midpalatal suture during rapid expansion in rats, Am. J. Orthod. Dentofacial Orthop. 154 (1) (2018) 115–127.
[21] G.H. Tang, J. Xu, R.J. Chen, Y.F. Qian, G. Shen, Lithium delivery enhances bone growth during midpalatal expansion, J. Dent. Res. 90 (3) (2011) 336–340.
[22] J.C. Danz, M. Dalstra, D.D. Bosshardt, C. Katsaros, A. Stavropoulos, A rat model for orthodontic translational expansive tooth movement, Orthod. Craniofac. Res. 16 (4) (2013) 223–233.
[23] B. Gaihre, S. Uswatta, A.C. Jayasuriya, Reconstruction of craniomaxillofacial bone defects using tissue-engineering strategies with injectable and non-injectable scaffolds, J. Funct. Biomater. 8 (4) (2017).
[24] M.B. Dreifke, N.A. Ebraheim, A.C. Jayasuriya, Investigation of potential injectable polymeric biomaterials for bone regeneration, J. Biomed. Mater. Res. 101 (8) (2013) 2436–2447.
[25] M. Terbish, S.H. Yoo, H.J. Kim, H.S. Yu, C.J. Hwang, H.S. Baik, J.Y. Cha, Accelerated bone formation in distracted alveolar bone after injection of recombinant human bone morphogenetic protein-2, J. Periodontol. 86 (9) (2015) 1078–1086.
[26] F. Tamimi, J. Torres, E. Lopez-Cabarcos, D.C. Bassett, P. Habibovic, E. Luceron, J. E. Barralet, Minimally invasive maxillofacial vertical bone augmentation using brushite based cements, Biomaterials 30 (2) (2009) 208–216.
[27] M. Yu, L. Ma, Y. Yuan, X. Ye, A. Montagne, J. He, T.V. Ho, Y. Wu, Z. Zhao, N. Sta Maria, R. Jacobs, M. Urata, H. Wang, B.V. Zlokovic, J.F. Chen, Y. Chai, Cranial suture regeneration mitigates skull and neurocognitive defects in craniosynostosis, Cell 184 (1) (2021) 243–256 e18.
[28] Y. Zhou, Y. Ni, Y. Liu, B. Zeng, Y. Xu, W. Ge, The role of simvastatin in the osteogenesis of injectable tissue-engineered bone based on human adipose-derived stromal cells and platelet-rich plasma, Biomaterials 31 (20) (2010) 5325–5335.
[29] Z. Yuan, P. Wei, Y. Huang, W. Zhang, F. Chen, X. Zhang, J. Mao, D. Chen, Q. Cai, X. Yang, Injectable PLGA microspheres with tunable magnesium ion release for promoting bone regeneration, Acta Biomater. 85 (2019) 294–309.
[30] R. Dimatteo, N.J. Darling, T. Segura, In situ forming injectable hydrogels for drug delivery and wound repair, Adv. Drug Deliv. Rev. 127 (2018) 167–184.
[31] M. Liu, X. Zeng, C. Ma, H. Yi, Z. Ali, X. Mou, S. Li, Y. Deng, N. He, Injectable hydrogels for cartilage and bone tissue engineering, Bone Res. 5 (2017) 17014.
[32] S. Hou, X. Niu, L. Li, J. Zhou, Z. Qian, D. Yao, F. Yang, P.X. Ma, Y. Fan, Simultaneous nano- and microscale structural control of injectable hydrogels via the assembly of nanofibrous protein microparticles for tissue regeneration, Biomaterials 223 (2019) 119458.
[33] G.C. Ingavle, M. Gionet-Gonzales, C.E. Vorwald, L.K. Bohannon, K. Clark, L. D. Galuppo, J.K. Leach, Injectable mineralized microsphere-loaded composite hydrogels for bone repair in a sheep bone defect model, Biomaterials 197 (2019) 119–128.
[34] J.H. Oh, H.J. Kim, T.I. Kim, J.H. Baek, H.M. Ryoo, K.M. Woo, The effects of the modulation of the fibronectin-binding capacity of fibrin by thrombin on osteoblast differentiation, Biomaterials 33 (16) (2012) 4089–4099.
[35] G. Giannini, V. Mauro, T. Agostino, B. Gianfranco, Use of autologous fibrin-platelet glue and bone fragments in maxillofacial surgery, Transfus. Apher. Sci. 30 (2) (2004) 139–144.
[36] A.S. Wolberg, Thrombin generation and fibrin clot structure, Blood Rev. 21 (3) (2007) 131–142.
[37] T. Burnouf, H.A. Goubran, T.M. Chen, K.L. Ou, M. El-Ekiaby, M. Radosevic, Blood-derived biomaterials and platelet growth factors in regenerative medicine, Blood Rev. 27 (2) (2013) 77–89.
[38] S. Padilla, M. Sanchez, G. Orive, E. Anitua, Human-based biological and biomimetic autologous therapies for musculoskeletal tissue regeneration, Trends Biotechnol. 35 (3) (2017) 192–202.
[39] C. Linsley, B. Wu, B. Tawil, The effect of fibrinogen, collagen type I, and fibronectin on mesenchymal stem cell growth and differentiation into osteoblasts, Tissue Eng. 19 (11–12) (2013) 1416–1423.
[40] L.A. McDuffee, B.P. Esparza Gonzalez, R. Nino-Fong, E. Aburto, Evaluation of an in vivo heterotopic model of osteogenic differentiation of equine bone marrow and muscle mesenchymal stem cells in fibrin glue scaffold, Cell Tissue Res. 355 (2) (2014) 327–335.
[41] L. Wang, C. Zhang, C. Li, M.D. Weir, P. Wang, M.A. Reynolds, L. Zhao, H.H. Xu, Injectable calcium phosphate with hydrogel fibers encapsulating induced pluripotent, dental pulp and bone marrow stem cells for bone repair, Mater. Sci. Eng. C Mater. Biol. Appl. 69 (2016) 1125–1136.
[42] A. Noori, S.J. Ashrafi, R. Vaez-Ghaemi, A. Hatamian-Zaremi, T.J. Webster, A review of fibrin and fibrin composites for bone tissue engineering, Int. J. Nanomed. 12 (2017) 4937–4961.

[43] J. Dong, G. Cui, L. Bi, J. Li, W. Lei, The mechanical and biological studies of calcium phosphate cement-fibrin glue for bone reconstruction of rabbit femoral defects, Int. J. Nanomed. 8 (2013) 1317–1324.
[44] M.A. Lopez-Heredia, J. Pattipeilohy, S. Hsu, M. Grykien, B. van der Weijden, S. C. Leeuwenburgh, P. Salmon, J.G. Wolke, J.A. Jansen, Bulk physicochemical, interconnectivity, and mechanical properties of calcium phosphate cements-fibrin glue composites for bone substitute applications, J. Biomed. Mater. Res. 101 (2) (2013) 478–490.
[45] F.A. van Esterik, B. Zandieh-Doulabi, C.J. Kleverlaan, J. Klein-Nulend, Enhanced osteogenic and vasculogenic differentiation potential of human adipose stem cells on biphasic calcium phosphate scaffolds in fibrin gels, Stem Cell. Int. 2016 (2016) 1934270.
[46] X. Yan, C. Yu, X. Zhou, J. Tang, D. Zhao, Highly ordered mesoporous bioactive glasses with superior in vitro bone-forming bioactivities, Angew. Chem. Int. Ed. 43 (44) (2004) 5980–5984.
[47] X. Yan, X. Huang, C. Yu, H. Deng, Y. Wang, Z. Zhang, S. Qiao, G. Lu, D. Zhao, The in-vitro bioactivity of mesoporous bioactive glasses, Biomaterials 27 (18) (2006) 3396–3403.
[48] J.R. Jones, L.M. Ehrenfried, L.L. Hench, Optimising bioactive glass scaffolds for bone tissue engineering, Biomaterials 27 (7) (2006) 964–973.
[49] S. Kargozar, M. Montazerian, S. Hamzehlou, H.W. Kim, F. Baino, Mesoporous bioactive glasses: promising platforms for antibacterial strategies, Acta Biomater. 81 (2018) 1–19.
[50] Z. Nescakova, K. Zheng, L. Liverani, Q. Nawaz, D. Galuskova, H. Kankova, M. Michalek, D. Galusek, A.R. Boccaccini, Multifunctional zinc ion doped sol - gel derived mesoporous bioactive glass nanoparticles for biomedical applications, Bioact. Mater. 4 (2019) 312–321.
[51] A. El-Fiqi, N. Mandakhbayar, S.B. Jo, J.C. Knowles, J.H. Lee, H.W. Kim, Nanotherapeutics for regeneration of degenerated tissue infected by bacteria through the multiple delivery of bioactive ions and growth factor with antibacterial/angiogenic and osteogenic/odontogenic capacity, Bioact. Mater. 6 (1) (2021) 123–136.
[52] L. Zhou, L. Fan, F.M. Zhang, Y. Jiang, M. Cai, C. Dai, Y.A. Luo, L.J. Tu, Z.N. Zhou, X.J. Li, C.Y. Ning, K. Zheng, A.R. Boccaccini, G.X. Tan, Hybrid gelatin/oxidized chondroitin sulfate hydrogels incorporating bioactive glass nanoparticles with enhanced mechanical properties, mineralization, and osteogenic differentiation, Bioact. Mater. 6 (3) (2021) 890–904.
[53] T. Xin, Y. Gu, R. Cheng, J. Tang, Z. Sun, W. Cui, L. Chen, Inorganic strengthened hydrogel membrane as regenerative periosteum, ACS Appl. Mater. Interfaces 9 (47) (2017) 41168–41180.
[54] K. Zheng, A.R. Boccaccini, Sol-gel processing of bioactive glass nanoparticles: a review, Adv. Colloid Interface Sci. 249 (2017) 363–373.
[55] M. Schumacher, P. Habibovic, S. van Rijt, Mesoporous bioactive glass composition effects on degradation and bioactivity, Bioact. Mater. 6 (7) (2021) 1921–1931.
[56] S. Abiraman, H.K. Varma, P.R. Umashankar, A. John, Fibrin glue as an osteoinductive protein in a mouse model, Biomaterials 23 (14) (2002) 3023–3031.
[57] C. Irgin, B. Corekci, F. Ozan, K. Halicioglu, O. Toptas, A. Birinci Yildirim, A. Turker, F. Yilmaz, Does stinging nettle (Urtica dioica) have an effect on bone formation in the expanded inter-premaxillary suture? Arch. Oral Biol. 69 (2016) 13–18.
[58] A.B. Altan, A.A. Bicakci, M.C. Avunduk, H. Esen, The effect of dosage on the efficiency of LLLT in new bone formation at the expanded suture in rats, Laser Med. Sci. 30 (1) (2015) 255–262.
[59] F. Ozan, B. Corekci, O. Toptas, K. Halicioglu, C. Irgin, F. Yilmaz, Y. Hezenci, Effect of Royal Jelly on new bone formation in rapid maxillary expansion in rats, Med. Oral Patol. Oral Cir. Bucal 20 (6) (2015) e651–e656.
[60] W. Jang, Y.J. Choi, S. Hwang, C.J. Chung, K.H. Kim, Anchorage loss assessment of the indirect anchor tooth during adjunctive orthodontic treatment, Am. J. Orthod. Dentofacial Orthop. 155 (3) (2019) 347–354.
[61] A.H. Jheon, S. Oberoi, R.C. Solem, S. Kapila, Moving towards precision orthodontics: an evolving paradigm shift in the planning and delivery of customized orthodontic therapy, Orthod. Craniofac. Res. 20 (Suppl 1) (2017) 106–113.
[62] L. Favero, P. Brollo, E. Bressan, Orthodontic anchorage with specific fixtures: related study analysis, Am. J. Orthod. Dentofacial Orthop. 122 (1) (2002) 84–94.
[63] K. Janssen, G. Raghoebar, A. Vissink, A.J. Sandham, Skeletal anchorage in orthodontics–a review of various systems in animal and human studies 23 (1) (2008) 75–88.
[64] M. Schatzle, R. Mannchen, M. Zwahlen, N.P. Lang, Survival and failure rates of orthodontic temporary anchorage devices: a systematic review, Clin. Oral Implants Res. 20 (12) (2009) 1351–1359.
[65] X. Yan, W. He, T. Lin, J. Liu, X. Bai, G. Yan, L. Lu, Three-dimensional finite element analysis of the craniomaxillary complex during maxillary protraction with bone anchorage vs conventional dental anchorage, Am. J. Orthod. Dentofacial Orthop. 143 (2) (2013) 197–205.
[66] B. Thiruvenkatachari, P. Ammayappan, R. Kandaswamy, Comparison of rate of canine retraction with conventional molar anchorage and titanium implant anchorage, Am. J. Orthod. Dentofacial Orthop. 134 (1) (2008) 30–35.
[67] Y. Zhu, S. Kaskel, Comparison of the in vitro bioactivity and drug release property of mesoporous bioactive glasses (MBGs) and bioactive glasses (BGs) scaffolds, Microporous Mesoporous Mater. 118 (1–3) (2009) 176–182.
[68] L.L. Hench Hench, J. Wilson, Surface-active biomaterials, Science 226 (4675) (1984) 630–636.
[69] I.D. Xynos, M.V. Hukkanen, J.J. Batten, L.D. Buttery, L.L. Hench, J.M. Polak, Bioglass 45S5 stimulates osteoblast turnover and enhances bone formation in vitro: implications and applications for bone tissue engineering, Calcif. Tissue Int. 67 (4) (2000) 321–329.
[70] I.D. Xynos, A.J. Edgar, L.D. Buttery, L.L. Hench, J.M. Polak, Ionic products of bioactive glass dissolution increase proliferation of human osteoblasts and induce insulin-like growth factor II mRNA expression and protein synthesis, Biochem. Biophys. Res. Commun. 276 (2) (2000) 461–465.
[71] I.D. Xynos, A.J. Edgar, M. Ramachandran, L.D.K. Buttery, L.L. Hench, Biochemical characterisation and gene expression profiling of human trabecular bone derived osteoblasts, J. Pathol. 193 (2001) 31A, 31A.
[72] I.D. Xynos, A.J. Edgar, L.D.K. Buttery, L.L. Hench, J.M. Polak, Gene-expression profiling of human osteoblasts following treatment with the ionic products of Bioglass (R) 45S5 dissolution, J. Biomed. Mater. Res. 55 (2) (2001) 151–157.
[73] P. Sepulveda Jones, L.L. Hench, Dose-dependent behavior of bioactive glass dissolution, J. Biomed. Mater. Res. 58 (6) (2001) 720–726.
[74] A. Haider, A. Waseem, N. Karpukhina, S. Mohsin, Strontium- and zinc-containing bioactive glass and alginates scaffolds, Bioengineering (Basel) 7 (1) (2020).
[75] A. Hoppe, N.S. Güldal, A.R. Boccaccini, A review of the biological response to ionic dissolution products from bioactive glasses and glass-ceramics, Biomaterials 32 (11) (2011) 2757–2774.
[76] I.A. Silver, J. Deas, M. Erecinska, Interactions of bioactive glasses with osteoblasts in vitro: effects of 45S5 Bioglass (R), and 58S and 77S bioactive glasses on metabolism, intracellular ion concentrations and cell viability, Biomaterials 22 (2) (2001) 175–185.
[77] S. Kargozar, F. Baino, S. Hamzehlou, R.G. Hill, M. Mozafari, Bioactive glasses: sprouting angiogenesis in tissue engineering, Trends Biotechnol. 36 (4) (2018) 430–444.
[78] A. Gorustovich, J. Roether, A. Boccaccini, Effect of bioactive glasses on angiogenesis: a review of in vitro and in vivo evidences, tissue engineering, Part B: Reviews 16 (2) (2010) 199–207.
[79] A. Leu, J.K. Leach, Proangiogenic potential of a collagen/bioactive glass substrate, Pharmaceut. Res. 25 (5) (2008) 1222–1229.
[80] J.M. Sadowska, M.P. Ginebra, Inflammation and biomaterials: role of the immune response in bone regeneration by inorganic scaffolds, J. Mater. Chem. B 8 (41) (2020) 9404–9427.
[81] L. Liu, F. Zhao, X. Chen, M. Luo, Z. Yang, X. Cao, G. Miao, D. Chen, X. Chen, Local delivery of FTY720 in mesoporous bioactive glass improves bone regeneration by synergistically immunomodulating osteogenesis and osteoclastogenesis, J. Mater. Chem. B 8 (28) (2020) 6148–6158.
[82] R.M. Day, A.R. Boccaccini, Effect of particulate bioactive glasses on human macrophages and monocytes in vitro, J. Biomed. Mater. Res. 73A (1) (2005) 73–79.
[83] M. Brennan Brennan, Fibrin glue, Blood Rev. 5 (4) (1991) 240–244.
[84] Vaquero, J. Vaquero, A. Arias, S. Oya, R. Martinez, M. Zurita, Effect of fibrin glue on postlaminectomy scar formation, Acta Neurochir. 120 (3–4) (1993) 159–163.
[85] M. Cekinmez, O. Sen, B. Atalay, B. Erdogan, M. Bavbek, H. Caner, O. Ozen, N. Altinors, Effects of methyl prednisolone acetate, fibrin glue and combination of methyl prednisolone acetate and fibrin glue in prevention of epidural fibrosis in a rat model, Neurol. Res. 32 (7) (2010) 700–705.
[86] X. Dong, J. Chang, H. Li, Bioglass promotes wound healing through modulating the paracrine effects between macrophages and repairing cells, J. Mater. Chem. B 5 (26) (2017) 5240–5250.
[87] H. Yu, J. Peng, Y. Xu, J. Chang, H. Li, Bioglass activated skin tissue engineering constructs for wound healing, ACS Appl. Mater. Interfaces 8 (1) (2016) 703–715.
[88] M. Montes-Casado, A. Sanvicente, L. Casarrubios, M.J. Feito, J.M. Rojo, M. Vallet-Regi, D. Arcos, P. Portoles, M.T. Portoles, An immunological approach to the biocompatibility of mesoporous SiO2-CaO nanospheres, Int. J. Mol. Sci. 21 (21) (2020).
[89] X. Chen, Z. Wang, N. Duan, G. Zhu, E.M. Schwarz, C. Xie, Osteoblast-osteoclast interactions, Connect. Tissue Res. 59 (2) (2018) 99–107.
[90] T.B. Huang, Y.Z. Li, K. Yu, Z. Yu, Y. Wang, Z.W. Jiang, H.M. Wang, G.L. Yang, Effect of the Wnt signal-RANKL/OPG axis on the enhanced osteogenic integration of a lithium incorporated surface, Biomater. Sci. 7 (3) (2019) 1101–1116.
[91] E. Rezende, V. Bradaschia-Correa, F. Siviero, L.M.B. Ambrosio, V.E. Arana-Chavez, Effects of bisphosphonates on osteogenesis and osteoclastogenesis signaling during the endochondral ossification of growing rats, Cell Tissue Res. 368 (2) (2017) 287–300.